Transrelativistic pair plasmas in AGN jets

M. Böttcher [1], M. Pohl [2], R. Schlickeiser [3]

ABSTRACT

Models of relativistic jets filled with ultrarelativistic pair plasma are very successful in explaining the broadband radiation of γ-ray blazars. Assuming that the initial injection and cooling of ultrarelativistic pair plasma in an AGN jet has occurred, producing the observed high-energy γ-ray radiation, we investigate the further evolution of the pair plasma as it continues to move out from the central engine. The effects of thermalization and reacceleration, the emission of pair bremsstrahlung and annihilation radiation and the bulk Compton process, and the possible application to MeV blazars are discussed. A model calculation to the special case of PKS 0208-512 is presented.

Subject headings: acceleration of particles — plasmas — radiation mechanisms: non-thermal — radiation mechanisms: thermal — radiative transfer — galaxies: jets — gamma-rays: theory

1. Introduction

The detection of high-energy γ-ray emission from more than 60 blazars with EGRET is a challenge and at the same time a constraint of fundamental importance for emission models (von Montigny et al. 1995). A large fraction of these blazars exhibits variability at γ-ray energies on time scales of days to months (Mukherjee et al. 1997). The optical counterparts of the majority of EGRET detected AGN are known as BL Lacertae objects and optically violent variable quasars (OVV). At radio wavelengths, all blazars can be recognized as bright, compact sources with a flat synchrotron spectrum emanating from outflowing plasma jets that are nearly aligned with our line-of-sight. Relativistic beaming is required in the objects in view of the luminosity and variability time scales (Dermer and Gehrels 1995), in accord with VLBI observations indicating

[1]Rice University, MS 108, Space Physics and Astronomy Department,
6100 S. Main Street, Houston, TX 77005 – 1892, USA; E-mail: mboett@spacsun.rice.edu
phone: (713) 527 8750 Ext. 2653, fax: (713) 285 5143

[2]Danish Space Research Institute, Juliane Maries Vej 30, DK – 2100 København Ø, Denmark

[3]Institut für Theoretische Physik, Lehrstuhl IV, Ruhr-Universität Bochum,
D – 44 780 Bochum, Germany

that superluminal motion is a common feature in this class of AGN (e.g. Wehrle et al. 1994, Pohl et al. 1995, Barthel et al. 1995, Krichbaum et al. 1995).

The strongest EGRET blazar detections can be characterized by a single power-law spectrum with differential photon spectral indices between $\alpha = 1.5$ and $\alpha = 2.7$ (Thompson et al. 1995). For individual sources the spectral index is correlated with the flux level, and there may also be deviations from the power-law behaviour both below 70 MeV and above a few GeV (Pohl et al. 1997). The combined OSSE/COMPTEL/EGRET measurements generally indicate spectral breaks at a few MeV (Williams et al. 1995, McNaron-Brown et al. 1995) in the sense that the spectra below 1 MeV are harder than in the EGRET range.

At medium γ-ray energies observable by COMPTEL, PKS 0208-512 has been identified as an AGN with flaring properties at MeV energies (Blom et al. 1995). There is now evidence that it may belong to a class of 'MeV-blazars' that are occasionally exceptionally bright MeV sources (see Bloemen et al. 1995). Since in these objects the bright emission appears to be confined to a relatively narrow energy range, the discussion has focused on models involving a broad blue-shifted e^+/e^- annihilation line that is Doppler boosted in a relativistic jet (Roland and Hermsen 1995). If this interpretation applies, MeV-blazars provide a unique tool to study astrophysical particle beams (e.g. Schlickeiser 1996). Furthermore, MeV-blazars may confuse the analysis of galactic sources of γ-ray line emission (Pohl 1996).

In an earlier paper (Böttcher, Mause & Schlickeiser 1997; hereafter BMS) we have investigated the temporal evolution of ultrarelativistic pair plasmas in jets of quasars and BL-Lac objects and have demonstrated that their broadband spectra can well be explained as the resulting synchrotron and inverse-Compton radiation from a cooling ultrarelativistic nonthermal pair plasma in a relativistic jet. A decisive parameter for the evolution of single ultrarelativistic plasma components inside an AGN jet is the density of pairs injected into the jet. Broadband fits, covering the radio to γ-ray regime of the electromagnetic spectrum, to blazars generally require particle densities of order $n_e \lesssim 10^3$ cm^{-3}. Nevertheless, fits to different objects suggest that the value of the pair density in relativistic jets ejected by active galactic nuclei varies over several orders of magnitude. Jets of very high density ($n \gtrsim 10^5$ cm^{-3}) can also produce the broadband spectra at least of γ-ray active flat-spectrum radio quasars whose bolometric luminosity is clearly dominated by the γ-ray emission.

In this paper, we argue that after an initial phase of rapid cooling, governed by synchrotron and inverse-Compton energy losses, the relativistic pair plasma inside such components is likely to attain a quasi-thermal distribution. If the jet remains well collimated and cooling (e. g. through adiabatic losses) remains very efficient through the transrelativistic phase, pair bremsstrahlung and pair annihilation become efficient. The resulting radiation spectrum peaks around several MeV, which has been suggested previously to be responsible for the observed MeV bump in MeV blazars (Henri et al. 1993, Roland & Hermsen 1995, Böttcher & Schlickeiser 1996). However, while generally the high-energy radiation from a few ultrarelativistic jet components,

ejected over the typical EGRET variability time scale, is appropriate to model EGRET spectra, the pair annihilation and bremsstrahlung radiation from only a few components after cooling and thermalization is usually too weak to explain the MeV blazar phenomenon. Therefore, a quasi-continuous supply of mildly relativistic pair plasma into the jet is required in order to fit the MeV bump in MeV blazars with pair annihilation radiation.

Alternatively, if very close to the central accretion disk the inverse-Compton cooling rate is balanced by reacceleration by hydromagnetic turbulences the pair plasma in the jet will thermalize at relativistic temperatures and will continuously Compton upscatter external radiation from the accretion disk very efficiently, producing another bump at keV — MeV energies by the so-called bulk Compton process (Sikora et al. 1997).

We know from the EGRET data of many blazars that the GeV emission is not that of a single injection of particles, but is more likely to result from more or less regularly repeating injection events with varying energy input into the ejected particles. A second important point is the correlation between flux and spectral index in the EGRET range. The spectral hardening during outbursts indicates a more efficient acceleration of particles. Even for highly variable sources like PKS 0208-512, PKS 0528+134 (Collmar et al. 1997) and others the low-energy γ-ray continuum varies with small amplitudes and not in phase with the variability in the EGRET range. To be more realistic we may thus either assume that injections occur in regular time intervals, so that they would not influence each other in their evolution, or that injection occurs in a quasi-steady manner, such that relativistic pair plasma is continuously injected.

For ease of both computing and exposition we will not consider the effect of the finite light travel time within the volume occupied by pair plasma, which limits our predictions of variability to time scales longer than the light travel time through individual plasma blobs. In section 2, we give a short overview of the different elementary processes which play a role for the evolution of a relativistic pair plasma component of an AGN jet after the initial phase of rapid cooling and which are usually not considered in models of ultrarelativistic jets. In section 3, we describe numerical simulations and an analytical approximation, applicable under special conditions, to follow the evolution of the pair plasma through the transrelativistic phase. We find that, depending basically on the particle density and the magnetic field, there are two different ways how a quasi-thermal distribution can be established. The relevant physics of these quasi-thermal plasmas is described in section 4. Section 5 contains a model calculation for the typical MeV blazar PKS 0208-512. We summarize in section 6.

2. The elementary processes

The momentum distribution of pairs inside a relativistic jet component is assumed to be isotropic and (for sake of simplicity) homogeneous. Under circumstances which will be specified below, the time evolution of such a pair plasma can be approached by a Fokker-Planck equation

regarding only time and particle energy as variables:

$$\frac{\partial}{\partial t}n(\gamma,t)+\frac{\partial}{\partial\gamma}\left[\left(\frac{d\gamma}{dt}\right)n(\gamma,t)\right]-\frac{1}{2}\frac{\partial^2}{\partial\gamma^2}\left[\frac{d\left(\Delta\gamma\right)^2}{dt}n(\gamma,t)\right]=\frac{d\,n(\gamma,t)}{dt}. \quad (1)$$

Here, $\frac{d\gamma}{dt}$ is the single-particle energy loss due to all the relevant elementary processes and $\frac{d(\Delta\gamma)^2}{dt}$ is the energy dispersion rate. The term on the right-hand sight of Eq. (1) is the source function. We restrict ourselves to the case where the plasma component is optically thin to γ-γ pair production (this process might well have led to re-injection of pairs during the ultrarelativistic phase but becomes irrelevant in the transrelativistic regime), and consider the catastrophic pair annihilation losses and the dilution of the blob due to expansion.

A detailed description of the calculation of the energy loss/gain rates due to inverse-Compton scattering of accretion disk radiation, synchrotron emission and the SSC process can be found in BMS. At the final states of the simulations carried out there, the particles have cooled down to energies such that all Compton scattering events may be treated in the Thomson regime. This guarantees that the use of the Fokker-Planck equation to describe the effect of inverse-Compton scattering is a good approach, which requires that the change in particle energy is $\Delta\gamma \ll \gamma - 1$ for each scattering event. Since $\Delta\gamma \lesssim \epsilon\,(\gamma^2-1) = \epsilon(\gamma+1)\,(\gamma-1)$ and $\epsilon\gamma \ll 1$, this condition is fulfilled in the case of Thomson scattering. The external photon source is assumed to be dominated by the accretion disk. The full angle-dependence of the accretion-disk photon field is included in our calculation.

Modelling of blazar spectra indicates that the magnetic fields in many AGN jets can be significantly lower than the equipartition value. Therefore, the gas pressure generally exceeds the magnetic pressure, leading to a conical jet and freely expanding blobs. The inferred low magnetic fields (typically $B \lesssim 0.1$ – 1 G) in some objects, together with the fact that the magnetic field generally declines outward, imply that synchrotron radiation (and therefore also reacceleration by synchrotron-self absorption) is of minor importance in the evolutionary phase with which we are dealing in this paper.

In ultrarelativistic jets, the effects of elastic (Møller and Bhabha) and inelastic scattering (pair bremsstrahlung emission), adiabatic losses, pair annihilation and stochastic reacceleration may be neglected compared to the dominant influence of synchrotron and inverse-Compton losses (BMS). Being interested in the details of the process of cooling down to mildly-relativistic energies, we now have to consider them and therefore discuss their influence in the following subsections. In this phase of the jet evolution, also the expansion of the jet will have a significant influence via adiabatic cooling and the dilution of the particle densities, affecting elastic and inelastic scattering and pair annihilation.

2.1. Elastic scattering

The energy loss/gain rate due to Møller scattering of electrons (positrons) of energy γ_t off an isotropic distribution $n_\pm(\gamma_\pm) = 4\pi N_\pm \beta_\pm \gamma_\pm^2 \, f_\pm(\gamma_\pm)$ of positrons (electrons) in the general case has been calculated by Dermer (1985). Here, we may restrict our considerations to the relativistic case in which the elementary single-particle energy loss is dominated by the term involving the Coulomb logarithm.

As was suggested by Nayakshin & Melia (1998), in this case the single-particle energy gain/loss rate reduces to a one-dimensional integral:

$$\frac{d\gamma_t}{dt} = \int_1^\infty d\gamma_2 \, n_\pm(\gamma_2) \, a(\gamma_t, \gamma_2) \tag{2}$$

where

$$a(\gamma_t, \gamma_2) = (\gamma_2 - \gamma_t) \, \frac{2\,\pi\, c\, r_e^2 \, A}{\gamma_t^2 \beta_t \, \gamma_2^2 \beta_2} \, \left[\gamma_r \beta_r - \frac{2}{\beta_r} + \mathrm{arcosh}\gamma_r \right]_{\gamma_r = \gamma_t\gamma_2(1-\beta_t\beta_2)}^{\gamma_t\gamma_2(1+\beta_t\beta_2)} \tag{3}$$

is the monoenergetic energy exchange rate. Here,

$$A = \ln\Lambda + \frac{1}{2}\ln(2e) \approx \ln\Lambda + 0.8466. \tag{4}$$

The Coulomb logarithm $\ln\Lambda$ is only weakly dependent on the electron and positron energies. In our numerical calculations, we use the constant value $A = 20$. The difference between Møller (electron-electron) and Bhabha (electron-positron) scattering only occurs in the terms neglected in the derivation of eq. (3) and is negligible in the case of relativistic pairs. The energy-exchange rate scales linearly with particle density and, for energies smaller than the average particle energy of the distribution, $\gamma < \langle\gamma\rangle$, it declines roughly as $d\gamma/dt \propto \gamma^{-1}$. It changes the sign at $\gamma = \langle\gamma\rangle$ and approaches a constant, negative value for $\gamma \gg \langle\gamma\rangle$.

In order to evaluate the energy dispersion due to elastic (Møller and Bhabha) scattering, we use the technique outlined by Dermer (1985), together with the idea of Nayakshin & Melia (1998) to consider scattering off monoenergetic distributions (for which the dispersion rate can be calculated analytically) and then averaging over the distributions of the background particles. In contrast to the technique of Dermer (1985), this requires only one numerical integration. The resulting expressions are given in Appendix A.1. The energy-dispersion rate also scales linearly with particle density and depends only weakly on the particle energy in the range $|\gamma - \langle\gamma\rangle| \ll \langle\gamma\rangle$. The Fokker-Planck equation (1) is only valid if the energy distribution is narrow in the above sense, because otherwise elastic scattering events between particles of very high and very low energies would lead to a considerable energy gain $\Delta\gamma \gtrsim \gamma$ of the low-energetic particle.

2.2. Bremsstrahlung emission

The general treatment of the pair bremsstrahlung process is very cumbersome and has been investigated in several papers by Haug, posing special interest on pair bremsstrahlung emission in thermal pair plasmas (Haug 1975, 1985a, 1985b). The importance of this radiation mechanism to the hard X-ray and γ-ray emission of relativistic jets in AGNs has been demonstrated by Böttcher & Schlickeiser (1995).

For the pair distributions considered in this paper, we may restrict ourselves to the ultrarelativistic limit using the differential pair bremsstrahlung cross section derived by Baĭer, Fadin & Khoze (1967). The bremsstrahlung energy-loss rate is calculated in Appendix A.2. Inspecting the function $\overline{K}$ given there, we find that the final-state averaged energy-loss of a test particle emitting bremsstrahlung photons is typically of the order $m_e c^2$ and thus, for relativistic particles the necessary condition $\Delta\gamma \ll \gamma - 1$ is fulfilled. The energy-loss rate has the same linear dependence on particle density as for elastic scattering and depends on particle energy as $-d\gamma/dt \propto \gamma^{1.1}$. It is only weakly dependent on the shape of the relativistic pair distribution.

2.3. Effects of jet expansion

For the parameter range under consideration in this paper, we expect the jet to expand freely. This yields a declining particle density as

$$n(t) = n_0 \left(\frac{z(t)}{z_0}\right)^{-2} \tag{5}$$

and

$$\left(\frac{dn(t)}{dt}\right)_{\rm exp} = -2\,\frac{n(t)}{z}\,c\,\beta_\Gamma\,\Gamma. \tag{6}$$

The expansion also leads to adiabatic losses due to the invariance of the magnetic flux through the particle orbits, $B\,r_L^2 = \text{const.}$, where r_L is the Larmor radius of a particle. This provides an additional energy-loss term, $\dot{\gamma} = \gamma\beta^2\,\dot{B}/(2\,B)$, depending on the z dependence of the magnetic field. In the case of a perfectly isotropized magnetic field, its evolution is given by $B(z) \propto z^{-2}$, while a purely transversal magnetic field evolves as $B(z) \propto z^{-1}$ (Blandford & Rees 1974, Blandford & Königl 1979). Since the degree of isotropization of the magnetic field is not well known, we parametrize the magnetic field dependence as

$$B(z[t]) = B_0 \left(\frac{z(t)}{z_0}\right)^{-b} \tag{7}$$

with $1 \le b \le 2$. This yields

$$\left(\frac{d\gamma}{dt}\right)_{\rm ad} = -\frac{b}{2}\,\frac{\gamma\beta^2}{z}\,\beta_\Gamma\,\Gamma\,c. \tag{8}$$

2.4. Stochastic acceleration by Alfvèn waves

In order to estimate the reacceleration and energy dispersion rate due to wave-particle interaction we will restrict our calculation to parallel, transverse plasma waves, i. e. $\mathbf{k} \parallel \mathbf{B}_0$ and $\mathbf{E}\perp\mathbf{B}_0$, in a pure pair plasma. Here, $\mathbf{k}$ is the wave vector, $\mathbf{E}$ is the polarization vector of the plasma wave and $\mathbf{B}_0$ is the background magnetic field.

According to the scenario of the formation of jet components, described in detail in BMS, the role of protons inside the jet may be neglected. In this scenario, the pairs are created as secondary particles in photo-pair and photo-pion production by relativistic protons accelerated in the accretion disk magnetosphere and will greatly outnumber the primary particles and carry the dominant fraction of the total energy transferred to particles, if the duty cycle of γ-ray emission is much less than unity. This pair population becomes unstable with respect to the excitation of various electromagnetic and electrostatic waves, resulting in an explosive event which ejects the ultrarelativistic pair plasma along an existing jet structure. This implies that the mechanism for acceleration of the protons during the quiescent phase by stochastic processes, ultimately leading to the production of the unstable pair plasma population, is of completely different nature than the mechanism which injects the pair plasma into the jet. The magnetic field and the level of turbulence during the latter phase, in turn, are in general drastically different from their values along the jet structure.

It is well-known that relativistic particles can only interact efficiently with the Alfvèn part of the plasma wave spectrum. For this reason, we neglect interaction with electron (positron) cyclotron waves. The relevant Fokker-Planck coefficients for the interaction of electrons with Alfvèn wave turbulences propagating through an electron-proton plasma have been investigated in detail by Schlickeiser (1989). Here, we generalize his calculation to the case of Alfvèn waves in a pair plasma. We assume that the Alfvèn waves have wave numbers k between

$$k_{min} = \frac{2\,\pi}{R_B} \qquad \text{and} \qquad k_{max} = \frac{\Omega_0}{v_a} \tag{9}$$

where R_B is the radius of the jet component, Ω_0 is the nonrelativistic gyrofrequency of electrons/positrons, and $v_a = B_0\sqrt{\langle\gamma\rangle}/\sqrt{8\pi m_e n_e}$ is the Alfvèn velocity in a relativistic pair plasma.

Eq. (9) certainly underestimates the minimum wave number since we assume the magnetic field to be ordered on smaller scales than R_B. It is especially the highest-energetic particles which interact with these longest waves. But for ultrarelativistic particles, synchrotron and inverse-Compton cooling is much more important than wave-particle interactions. Thus, the

inaccuracy of Eq. (9) does not influence our final results. We assume that the spectral energy content in plasma waves is distributed according to a power-law,

$$I(k) = I_0\, k^{-q} \tag{10}$$

with

$$I_0 = 4\,\pi\,\left(\frac{\delta B}{B_0}\right)^2 \frac{B_0^2}{8\,\pi}\frac{q-1}{k_{min}^{1-q} - k_{max}^{1-q}}. \tag{11}$$

Here, δB is the amplitude of the magnetic field fluctuation due to the plasma waves which is typically of order $\lesssim 10^{-1}\, B_0$. Now, following the calculations of Schlickeiser (1989) (accounting for the differences of the dispersion relation between an e^--p- and an e^--e^+-plasma), we find the acceleration rate due to Alfvèn waves,

$$\left(\frac{d\gamma}{dt}\right)_A = \frac{\pi\,(q-1)}{q}\Omega_0^{2-q} k_{min}^{q-1}\,\left(\frac{\delta B}{B_0}\right)^2\, v_a^2\, c^{q-3}\,(\gamma\beta)^{q-1}, \tag{12}$$

and the energy dispersion rate

$$\left(\frac{d[\Delta\gamma]^2}{dt}\right)_A = 2\,\frac{\pi\,(q-1)}{q\,(q+2)}\Omega_0^{2-q} k_{min}^{q-1}\,\left(\frac{\delta B}{B_0}\right)^2\, v_a^2\, c^{q-3}\,\gamma^q\,\beta^{q+1}. \tag{13}$$

2.5. Energy dispersion due to inverse-Compton scattering

Being a stochastic process, also inverse-Compton scattering leads to energy dispersion. The respective energy-dispersion rates for Compton scattering in the Thomson regime are calculated in Appendix A.3.

For relativistic particles, the energy-dispersion rate due to inverse-Compton scattering is $d(\Delta\gamma)^2/dt \propto \gamma^4$ and linearly dependent on $\int_0^\infty d\epsilon\,\epsilon^2\, n_{ph}(\epsilon)$, i. e. the photon densities and the average of the square of the photon energies. Their extremely strong dependence on particle energy ($\propto \gamma^2$ and $\propto \gamma^4$, respectively) implies that the energy-exchange and dispersion rates due to inverse-Compton scattering will usually dominate the total rates for very high particle energies.

Which process is dominant at low particle energies, depends critically on the particle density and the strength of magnetohydrodynamic turbulences. In the case of high densities, elastic scattering will govern the evolution of these particles, while in the case of lower density and strong plasma wave turbulences, wave-particle interactions (reacceleration) and adiabatic losses will dominate their behavior.

Figs. 1 and 2 show the energy-exchange and energy-dispersion rates for the different processes for a plasma of density $3 \cdot 10^6\,\mathrm{cm}^{-3}$, having a narrow distribution around $\langle\gamma\rangle \approx 30$. A magnetic field of $B = 0.1$ G is assumed and the blob is located at $z = 10^{-3}$ pc above an accretion disk

with total luminosity $L = 10^{45}\,\mathrm{erg\,s^{-1}}$ and moves outward with bulk Lorentz factor $\Gamma = 15$. The magnetic-field is assumed to be isotropized ($b = 2$). These parameter values are similar to those which result from the cooling of an ultrarelativistic pair plasma producing an X-ray and γ-ray spectrum consistent with the observed spectrum of PKS 0208-512.

2.6. Pair annihilation losses

A detailed discussion of the effects of pair annihilation on a relativistic pair plasma in AGN jets can be found in Böttcher & Schlickeiser (1996). In order to calculate the total pair annihilation rate, we use the expression given by Svensson (1982) which, for completeness, is quoted in Appendix A.4. For relativistic particles, it declines roughly as $\dot{n}_{\pm}(\gamma_{\pm}) \propto (\gamma_{\pm}\langle\gamma_{\mp}\rangle)^{-1}$, where $\langle\gamma_{\mp}\rangle$ is the average Lorentz factor of electrons or positrons, respectively, and becomes only important in the case of very high particle densities.

3. Simulations of the jet evolution

Since several energy loss and dispersion rates depend on the present particle distributions, Eq. (1) in its general form represents a set of coupled integro-differential equations which, in general, can not be be solved analytically. For the purpose of numerical integration, we used an explicit code of finite differencing. Because the numerical simulations are extremely time-consuming we tried to find simplified approximative expressions for the coefficients in Eq. (1) in a way that the problem could be solved analytically. This is possible if both the cooling rate and the energy-dispersion rate are dominated by inverse-Compton scattering for all occupied energy states, which is the case if the pair distributions still have a relativistic low-energy cutoff at $\gamma \gtrsim 10$. Then pair annihilation is negligible and provided that the cooling time scale is much shorter than the time scale of dilution of the pair plasma due to expansion, the source term in Eq. (1) may be neglected. Furthermore, the energy-loss and dispersion coefficients are dominated by synchrotron emission and inverse-Compton scattering and can very well be approximated by

$$\frac{d\gamma}{dt} \approx -A_1\,\chi(t)\,\gamma^2, \tag{14}$$

$$\frac{d(\Delta\gamma)^2}{dt} \approx A_2\,\chi(t)\,\gamma^4 \tag{15}$$

where A_i are constants and both Fokker-Planck coefficients have the same explicit time dependence $\chi(t)$. For the resulting differential equation we found an approximative analytical solution which is derived in Appendix B. Given a known distribution $n(\gamma_0, 0)$ at $t = 0$, we can forward it in time to $t = t_1$ by

$$n(\gamma, T_1) = \frac{e^{\frac{A_1}{A_2\gamma} - \frac{A_1^2}{2A_2} T_1}}{2\,\gamma^3\,\sqrt{\pi\,A_2\,T_1/2}} \int_1^\infty d\gamma_0\, n(\gamma_0, 0)\, \gamma_0\, e^{-\frac{A_1}{A_2\gamma_0}}\, e^{-\left(\frac{1}{\gamma_0} - \frac{1}{\gamma}\right)^2 / (2\,A_2\,T_1)} \tag{16}$$

where

$$T := \int_0^t dt'\, \chi(t'). \tag{17}$$

Since the explicit time dependence $\chi(t)$ of the coefficients, being governed by the evolution of the dominant soft photon field, is difficult to separate in realistic situations, we choose time steps t_1 in a way that we may assume the coefficients $A_1\chi(t)$ and $A_2\chi(t)$ to be constant within this time interval, i. e. we approximate $\chi(t)$ by a step function. We use the solution (16) as long as the exact energy loss and dispersion rates of the lowest-energetic particles do not deviate more than 10 % from the representations (14) and (15). Comparison with numerical integrations of Eq. (1) showed good agreement. After this phase we continue with numerical integrations of the full Fokker-Planck equation.

It is obvious that we cannot extend the simulations using the code described above to subrelativistic pair temperatures since especially the bremsstrahlung cross section which we use is only valid in the ultrarelativistic limit. However, under a wide range of assumptions, the pair plasma attains a quasi-thermal distribution whose temperature depends basically on the energy density of the external radiation field, the pair density, the magnetic field and the amplitude of plasma wave turbulences.

Figs. 3 — 6 show two examples of this evolution as results of the numerical scheme described above. These examples illustrate the general tendency towards the establishment of a quasi-thermal distribution inside the jet component. At high particle energies the real quasi-equilibrium distributions are truncated, if radiative energy-loss processes dominate over adiabatic losses (Fig. 4). If adiabatic losses dominate, the high-energy end of the particle spectrum tends to be slightly harder than a thermal distribution (Fig. 6). In both examples, the initial conditions were chosen in a way that the γ-ray compactness is low, which results in a time-averaged power-law γ-ray spectrum of photon number index $\alpha_\gamma = (s+2)/2$ due to inverse-Compton scattering of soft photons, where s is the spectral index of the electron energy distribution.

In the case of extremely high particle densities ($n \gtrsim 10^8$ cm^{-3}), quasi-thermalization is a consequence of elastic scattering becoming the dominant energy exchange process. One example for this fact is illustrated in Figs. 3 and 4. Fig. 4 demonstrates that for such high densities, the truncation of the distribution functions with respect to a thermal distribution at high energies is of minor importance.

For the case of lower densities, Schlickeiser (1985) demonstrated that if the spectral index q of the Alfvèn wave turbulence equals 2, the combined action of stochastic acceleration and radiative

losses also establishes a quasi-thermal distribution. Its temperature is given by

$$\Theta = \sqrt{1 + (3+a)^2 \tilde{p}_c^2} - 1 \tag{18}$$

where $\tilde{p}_c\, m_e c$ is the particle momentum for which the net energy loss or gain, respectively, vanishes, and $a = \alpha_1/\alpha_2$ is the ratio of the coefficients governing the stochastic acceleration and energy-dispersion rates via $dp/dt = \alpha_1 p$ and $d(\Delta p)^2/dt = \alpha_2 p^2$. The equilibrium temperature in Eq. (18) obviously depends very sensitively on the efficiency of radiative cooling and can become quite high if the external photon energy density is low, because the energy dependence of adiabatic ($\propto \gamma$) and bremsstrahlung ($\propto \gamma^{1.1}$) energy losses is much weaker than that of inverse-Compton losses, leading to a very high equilibrium Lorentz factor (obviously, elastic-scattering [$\approx$ const.] cannot balance acceleration at all).

In our simulations, we find a similar behavior also for the case of Kolmogorov turbulence, i. e. for $q = 5/3$. Figs. 5 and 6 illustrate one example of this evolution. In this case, however, the deviation from a maxwellian distribution at high energies is more pronounced than in the case of a dense plasma. Assuming that inverse-Compton scattering of accretion disk radiation is the dominant cooling mechanism, which is balanced by stochastic reacceleration, and that quasi-thermalization occurs at relativistic temperatures, $\Theta \gg 1$, we find for the quasi-equilibrium temperature

$$\Theta_{eq} \approx 3 \cdot 10^5\, B_0^7\, R_{15}^{-2}\, n_e^{-3}\, \delta_{-1}^6\, \frac{z_{pc}^6}{L_{46}^3}, \tag{19}$$

where B_0 is the magnetic field in Gauss, R_{15} is the blob radius in units of 10^{15} cm, n_e is in cm^{-3}, $(\delta B/B_0) = 0.1\,\delta_{-1}$, $z_{pc} = z/(1\,\mathrm{pc})$, and $L_{46} = L_D/(10^{46}\,\mathrm{erg\,s^{-1}})$. In order to derive this estimate, we have used Eqs. (32), (37) and (38) in the limit $\Theta \gg 1$.

The X-ray and γ-ray emission of a quasi-thermal, mildly relativistic plasma is dominated by its pair annihilation and pair bremsstrahlung radiation. For pair temperatures $\Theta \lesssim 3$ the radiative output near the high-energy cut-off of the photon spectra is dominated by pair annihilation radiation which is insensitive to the pair distribution near its high-energy tail. The X-ray spectrum, to which only pair bremsstrahlung radiation contributes significantly and which has a photon number spectral index of $\alpha \approx 1.1$, is equally insensitive to the detailed shape of the pair distribution at high energies. For this reason, the observeable radiation from a mildly relativistic quasi-thermal pair plasma may well be approximated by the respective emission of a thermal plasma whose distribution coincides with the exact one up to the mean particle energy.

This situation changes if the plasma maintains a highly relativistic temperature ($\Theta \gtrsim 5$). In this case, the luminosities in synchrotron, SSC, and/or external Compton radiation may well dominate over pair bremsstrahlung and pair annihilation radiation, and the exact pair distribution has to be used in order to calculate the emitted X-ray and γ-ray spectrum.

The pair annihilation rate in a thermal plasma can be aproximated by

$$\frac{\partial n}{\partial t} = -\frac{2\,\pi\,c\,r_e^2\,n^2}{(1+\Theta)}\,\left(\frac{1}{1+6\Theta}+\frac{\Theta}{0.25+\ln(1+1.1545\Theta)}\right)^{-1} \tag{20}$$

(Svensson 1982). The bremsstrahlung emission of a thermal pair plasma can be calculated as

$$\dot{n}_{br}(k) = \sqrt{\frac{2}{3\,\pi}}\frac{2\,c\,\alpha\,\sigma_T\,n^2}{k\,\sqrt{\Theta}}e^{-k/\Theta}g(k,\Theta) \tag{21}$$

where $g(k,\Theta)$ are the respective gaunt factors for e-e and e^+-e^- bremsstrahlung for which we use the approximations for transrelativistic pair plasmas found by Skibo et al. (1995). The pair annihilation spectrum emitted by a thermal plasma is

$$\dot{n}_{ann}(k) = \frac{c\,n^2}{\Theta K_2^2\left(\frac{1}{\Theta}\right)}e^{-(2\,k^2+1)/(2\,k\,\Theta)}\int\limits_1^\infty d\gamma_r\,(\gamma_r-1)\,e^{-\gamma_r/(2\,k\,\Theta)}\sigma(\gamma_r) \tag{22}$$

(Dermer 1984) where

$$\sigma(\gamma_r) = \frac{\pi\,r_e^2}{1+\gamma_r}\,\left[\left(\frac{\gamma_r^2+4\gamma_r+1}{\gamma_r^2-1}\right)\ln\left(\gamma_r+\sqrt{\gamma_r^2-1}\right)-\frac{\gamma_r+3}{\sqrt{\gamma_r^2-1}}\right]. \tag{23}$$

The bulk Compton process is calculated in the Thomson regime, including the full angle-dependence of the external radiation field (see BMS for details).

We will now derive an estimate for the density required for elastic scattering to dominate the effect of stochastic reacceleration. To this aim, we compare the energy-loss due to elastic scattering for particles of energy $\gamma \gg \langle\gamma\rangle$ to the respective reacceleration rate. Using Eq. (2), we find

$$\left(\frac{d\gamma}{dt}\right)_{Mo,\gamma\gg\langle\gamma\rangle} \approx 6\cdot 10^{-9}\,\frac{n_4}{\langle\gamma\rangle}\,\mathrm{s}^{-1} \tag{24}$$

where $n_4 = n_e/(10^4\,\mathrm{cm}^{-3})$. The stochastic acceleration rate according to Eq. (12) is

$$\left(\frac{d\gamma}{dt}\right)_A \approx 5\cdot 10^{-2}\,B_0^{7/3}\,\delta_{-1}^2\,n_4^{-1}\,R_{15}^{-2/3}\,\langle\gamma\rangle^{-1}\,\gamma^{2/3}\,\mathrm{s}^{-1}. \tag{25}$$

This yields the condition

$$n_e \gtrsim 3\cdot 10^7\,B_0^{7/6}\,\delta_{-1}\,R_{15}^{-1/3}\,\gamma^{1/3}\,\mathrm{cm}^{-3} \tag{26}$$

for elastic scattering to dominate the energy loss at particle energy $\gamma \gg \langle\gamma\rangle$. If this condition is fulfilled for particles at the high-energy tail of the pair distribution, reacceleration is inefficient as compared to elastic scattering. In this case, radiative and adiabatic cooling will prevent the particle distributions from attaining a stationary state.

4. Evolution of a thermal plasma

As we have shown in Section 3, in the case of very high particle densities ($n \gtrsim 10^8$ cm^{-3}), the pair plasma of a relativistic jet component approaches a quasi-thermal distribution due to the dominant action of elastic scattering. The evolution of a thermal distribution of particles, subject to pair annihilation, bremsstrahlung, inverse-Compton, synchrotron, SSC, and adiabatic losses, can be followed using the expressions for the respective cooling rates of thermal pair plasmas.

For this purpose, we assume that the thermalization timescale (due to elastic scattering) is much shorter than the energy loss timescale. In this case, Møller and Bhabha scattering will always establish a thermal distribution,

$$dn(\gamma) = \frac{n\,\beta\gamma^2}{\Theta\,K_2\left(\frac{1}{\Theta}\right)} e^{-\frac{\gamma}{\Theta}}\,d\gamma, \tag{27}$$

where $\Theta = \frac{k_B T}{m_e c^2}$ is the dimensionless temperature and K_2 is the modified Bessel function of second kind of order 2. In order to determine the respective cooling rates in a thermal plasma, we note first that

$$\left\langle p^2 \right\rangle = (m_e c)^2 \left\langle \gamma^2 - 1 \right\rangle = (m_e c)^2 \cdot 3\,\Theta \frac{K_3\left(\frac{1}{\Theta}\right)}{K_2\left(\frac{1}{\Theta}\right)} \tag{28}$$

where $\langle . \rangle$ denotes the average over the distribution (27). Let $W = \frac{1}{n}\frac{dE}{dV}$ be the average particle energy. Then, the cooling rate due to synchrotron losses is

$$\left(\frac{\partial W}{\partial t}\right)_{\rm SY} \approx -c\,\sigma_T \frac{B^2}{2\,\pi}\,\Theta \frac{K_3\left(\frac{1}{\Theta}\right)}{K_2\left(\frac{1}{\Theta}\right)} e^{-\frac{\gamma_R}{\langle\gamma\rangle}} \tag{29}$$

where the exponential is an approximate expression to include the suppression of cooling due to the Razin-Tsytovich effect. $\langle\gamma\rangle = K_3(1/\Theta)/K_2(1/\Theta) - \Theta$ is the mean Lorentz factor of the pairs (see eq. [38]) and

$$\gamma_R \approx 2.1 \cdot 10^{-3} \left(\frac{n}{\rm cm^{-3}}\right)^{\frac{1}{2}} \left(\frac{B}{\rm G}\right)^{-1} \langle\gamma\rangle^{-\frac{1}{2}} \tag{30}$$

is the Razin-Tsytovich Lorentz factor (Crusius & Schlickeiser 1988). The cooling rate due to inverse-Compton scattering of accretion disk photons in the Thomson limit is

$$\left(\frac{\partial W}{\partial t}\right)_{\rm IC} = -m_e c^2\,\frac{4}{15}\frac{\pi^5\,\sigma_T}{c^2}\,\Gamma^2 \left(\frac{m_e c^2}{h}\right)^3 \Theta\,\frac{K_3\left(\frac{1}{\Theta}\right)}{K_2\left(\frac{1}{\Theta}\right)} \int\limits_{R_{in}}^{R_{out}} dR\,R\,\Theta_D^4(R)\,\frac{(x-\beta_\Gamma z)^2}{x^4} \tag{31}$$

where R is the distance of a point in the accretion disk to the centre, R_{in} and R_{out} are the boundary radii of the disk, $\Theta_D(R)$ is the dimensionless temperature of the accretion disk material at radius R, and $x = \sqrt{R^2 + z^2}$. If the point source approximation ($z \gg R_{out}$) holds, Eq. (31) reduces to

$$\left(\frac{\partial W}{\partial t}\right)_{\rm IC} = -\frac{\sigma_T\, L_0\, \Theta}{\pi\, \Gamma^2 (1+\beta_\Gamma)^2 z(t)^2} \frac{K_3\left(\frac{1}{\Theta}\right)}{K_2\left(\frac{1}{\Theta}\right)}. \tag{32}$$

Fig. 7 illustrates that for a typical Shakura-Sunyaev disk of total luminosity $L = 10^{46}$ erg s^{-1}, surrounding a black hole of mass $M = 10^8\, M_\odot$, the point source approximation is an appropriate choice for $z \geq 0.1$ pc. The temperature ($\Theta = 2$ in Fig. 7) enters both Eqs. (31) and (32) in the same way and does therefore not have any influence on the validity of the point source approximation.

The cooling rate due to pair bremsstrahlung emission of a thermal pair plasma has been calculated by Haug (1985b). We interpolate between his expressions for the extreme-relativistic and the non-relativistic regime:

$$-\left(\frac{\partial W}{\partial t}\right)_{\rm br} = \begin{cases} \frac{128}{3\sqrt{\pi}}\, \alpha r_e^2\, m_e c^3\, n \sqrt{\Theta} & \text{for } \Theta \ll 1, \\ 96\, \alpha\, r_e^2\, m_e c^3\, n\, \Theta\, (\ln(2\Theta) + 0.673) & \text{for } \Theta \gtrsim 1. \end{cases} \tag{33}$$

For synchrotron-self-Compton scattering, we approximate the synchrotron radiation field to be distributed over a small range of energies and use its energy density

$$u_{sy} = \frac{3\, R_B\, n}{4\, c} \left|\frac{\partial W}{\partial t}\right|_{SY} \tag{34}$$

leading to

$$\left(\frac{\partial W}{\partial t}\right)_{\rm SSC} = -\frac{4}{3} c \sigma_T\, u_{sy}\, \frac{\langle \gamma^2 - 1 \rangle}{n} = -\frac{3}{2} \frac{c\, \sigma_T^2\, R_B\, n\, B^2}{\pi}\, \Theta^2 \left(\frac{K_3\left[\frac{1}{\Theta}\right]}{K_2\left[\frac{1}{\Theta}\right]}\right)^2 e^{-\frac{\gamma_R}{\langle\gamma\rangle}}. \tag{35}$$

Using Eq. (8) for the adiabatic cooling rate, we find

$$\left(\frac{\partial W}{\partial t}\right)_{\rm ad} = -\frac{3}{2}\, m_e c^2\, b\, c\, \frac{\beta_\Gamma\, \Gamma}{z}\, \Theta. \tag{36}$$

The heating rate due to stochastic interactions with Alfvèn waves, according to Eq. (12), is

$$\left(\frac{\partial W}{\partial t}\right)_A = m_e c^2\, \sqrt{\pi}\, \frac{q-1}{q+2}\, \frac{\Gamma\left(\frac{q+4}{2}\right)}{q}\, 2^\nu\, \Theta^{\nu-2}\, \frac{K_\nu\left(\frac{1}{\Theta}\right)}{K_2\left(\frac{1}{\Theta}\right)}\, \Omega_0^{2-q}\, k_{min}^{q-1} \left(\frac{\delta B}{B_0}\right)^2 v_a^2\, c^{q-3} \tag{37}$$

where $\nu = (q+3)/2$.

The mean kinetic energy of the electrons and positrons in a thermal plasma of temperature Θ is

$$W_{\rm th} = \frac{m_e c^2}{\Theta\, K_2\left(\frac{1}{\Theta}\right)} \int_0^\infty d\gamma\,(\gamma-1)\,\gamma\sqrt{\gamma^2-1}\; e^{-\frac{\gamma}{\Theta}} = m_e c^2 \left(\frac{K_3\left[\frac{1}{\Theta}\right]}{K_2\left[\frac{1}{\Theta}\right]} - \Theta - 1\right) \tag{38}$$

(which in the non-relativistic limit approaches $W_{th} = m_e c^2\left[\frac{3}{2}\Theta + \frac{15}{2}\Theta^2\right]$). Thus,

$$\frac{\partial\Theta}{\partial W} = \frac{1}{m_e c^2}\left(-1 + \frac{1}{\Theta^2} + \frac{5}{\Theta}\frac{K_3\left[\frac{1}{\Theta}\right]}{K_2\left[\frac{1}{\Theta}\right]} - \left[\frac{K_3\left(\frac{1}{\Theta}\right)}{\Theta\, K_2\left(\frac{1}{\Theta}\right)}\right]^2\right)^{-1}, \tag{39}$$

and the respective cooling rates are determined by

$$\frac{\partial\Theta}{\partial t} = \frac{\partial\Theta}{\partial W}\cdot\frac{\partial W}{\partial t}. \tag{40}$$

The annihilation rate in a thermal plasma is well approximated by Eq. (20). We found that numerical solutions of the Fokker-Planck equation in the case of a thermal pair plasma are in good agreement with the calculation described in this section as long as the pair temperature is $\Theta \gtrsim 4$. At lower temperatures cooling of the thermal plasma is slower than predicted by our Fokker-Planck treatment. We attribute this mainly to the ultrarelativistic approximation used for the pair bremsstrahlung process which is not an appropriate approach for mildly relativistic temperatures.

In Fig. 8, we show three examples of the evolution of a thermal pair plasma in an AGN jet with different initial densities. Plasmas of very high density end up with a density evolution which is almost independent of density, since initially the density evolution is dominated by pair annihilation losses which are proportional to the square of the density. At lower densities, the dilution of the plasma due to the expansion of the jet always dominates the decline of the density, which thus always remains well below the density of a plasma injected with high initial density. The temperature evolution depends only weakly on the density because it is governed by adiabatic losses. The differences in the temperature evolution curves are a consequence of the density dependence of bremsstrahlung losses and of the heating rate via $v_a^2 \propto n^{-1}$.

The x-ray and γ-ray emission of a dense, mildly relativistic pair plasma in the outer parts of an AGN jet is calculated in the same way as for the dilute thermalized pair plasma, as described at the end of the previous section.

5. Application to PKS 0208-512

The quasar PKS 0208-512 is the most prominent example of MeV blazars, i. e. blazars exhibiting variable emission around several MeV and reaching extremely high fluxes in this frequency range, often dominating the total energy output of the source. Analyzing COMPTEL data of Phase I and II, Blom et al. (1995) found that during Phase I, PKS 0208-512 did not show a significant signal in the COMPTEL energy range, while in Phase II, a pronounced bump at 1 – 3 MeV was detected. Quasi-simultaneous EGRET observations revealed a strong signal from PKS 0208-512 during both Phase I and II. However, in Phase II, EGRET detected the source with lower significance than during Phase I. The EGRET spectra appear to be harder during Phase I than in Phase II. During Phase III PKS 0208-512 is again detected by EGRET at a high flux level, whereas the COMPTEL data for that period do not show evidence for emission from PKS 0208-512 (Blom 1996). The variability in the EGRET range correlates with spectral index, which itself varies more strongly than in the case of the average blazar (see Stacy et al. 1996 and Pohl et al. 1997). In fact, the flux level at 100 MeV stays approximately constant while the emission above 300 MeV is highly variable.

The variability timescale of the high-energy component of the γ-ray spectrum of our model system is determined by the light travel time through the plasma component and corresponds to ~ 6 h in the observer's frame. The timescales of quasi-thermalization and of dilution of the pair plasma due to pair annihilation and the expansion of the jet are of the order of a few weeks. An outburst at MeV energies due to transrelativistic, quasi-thermalizing pair plasma in a relativistic jet is therefore generally not expected to be correlated with a γ-ray outburst observed by EGRET within the same observing period. In general terms, the flux in the EGRET range reflects the injection rate of high-energy pairs, whereas the flux of X-ray and soft γ-ray photons is a measure of the injection rate of pairs at all energies averaged over several weeks.

The instantaneous pair annihilation and pair bremsstrahlung radiation of one single thermalizing pair plasma blob is too weak to produce the observed MeV bump in the spectrum of PKS 0208-512. Therefore, if the MeV blazar phenomenon is to be explained by pair annihilation radiation of cooled, thermalized pair plasma in a relativistic jet, this jet must be quasi-continuously filled with pair plasma.

If, in contrast, the MeV bump is produced by inverse Compton scattering of external radiation by the quasi-thermal, transrelativistic pair plasma in the jet, reacceleration of particles must be efficient because else the X-ray and soft γ-ray spectrum would just be the extension of the γ-ray power-law, resulting from Comptonization of soft radiation in the Compton-cooled nonthermal plasma. The bulk Compton process is therefore mainly relevant in the low to medium density case, in which relativistic temperatures can be maintained. However, a problem with this interpretation is that the quasi-equilibrium temperature of the pair plasma depends extremely sensitively on the magnetic field strength, the level of hydromagnetic turbulence and the injection height of the plasma blob, as indicated by Eq. (19). Therefore, if inverse-Compton scattering of external

radiation by quasi-thermal pair plasma in the jet plays an important role, we would expect to see bulk-Compton bumps in different objects at a largely different frequencies, for which no evidence has yet been found. There is no obvious reason why this bump should be produced preferrably at several MeV.

The dashed line in Fig. 9 shows a fit to the EGRET spectrum during Phase II (VP 220) where we adopted the following set of parameters: $n_e = 5 \cdot 10^5\,\mathrm{cm}^{-3}$, $R_B = 6 \cdot 10^{15}$ cm, $\gamma_{1\pm} = 500$, $\gamma_{2\pm} = 2 \cdot 10^4$, $s = 2.4$, $B_0 = 0.7$ G, $b = 2$, $z_i = 2 \cdot 10^{-3}$ pc, $\Gamma = 10$, $\theta_{obs} = 6°$, $L_0 = 10^{46}\,\mathrm{erg\,s}^{-1}$, $M_0 = 10^8\,M_\odot$. The high-energy spectrum results predominantly from inverse-Compton scattering of external (accretion-disk) photons. The photon spectrum has been integrated over the cooling time of the ultrarelativistic pair population because this time is only several hundred seconds (in the observer's frame) which cannot be resolved by COMPTEL and EGRET. The fluence resulting from our time integration has been re-converted into an average flux by multipling by the repetition rate of subsequent blobs. Since during an observed time interval Δt_{obs} the blob travels a distance $\Delta l = D\,\Gamma\,\beta_\Gamma\,c\,\Delta t_{\rm obs}$ cm, a jet filled quasi-continuously with relativistic material ($\Delta l \approx R_B$) corresponds to a repetition time in the observer's frame of $\Delta t_{\rm obs} \approx 2000$ s which translates to a quasi-continuous energy input into the jet of $L_{jet} \approx 5 \cdot 10^{43}$ erg s^{-1} during an EGRET outburst.

The bump of the radiation from an accretion disk of $L = 10^{46}$ erg s^{-1} at redshift $z \approx 1$ corresponds to $\nu\,F_\nu \approx 10^{-6}\,\mathrm{MeV\,cm^{-2}\,s^{-1}}$, if we assume $H_0 = 75\,\mathrm{km/(s \cdot Mpc)}$, $q_0 = 0.5$. No simultaneous broadband measurements in the radio to UV frequency range are available. For this reason, we make no attempt to fit the synchrotron component. Anyway, the radio emission probably originates in a much larger volume than considered here, in accord with the fact that there is no correlation between the simultaneously observed gamma-ray flux and cm-radio flux of blazars (Mücke et al. 1996, 1997).

Using the methods described in the previous sections, we follow the evolution of the plasma blob through the transrelativistic phase until it is diluted by pair annihilation and the expansion of the jet to less than 10^{-4} of its initial density. Due to the rather low initial density, quasi-thermalization occurs at a temperature of $\Theta \approx 100$, implying that the X-ray and soft γ-ray spectrum is strongly dominated by inverse Compton scattering of accretion disk radiation.

In order to reproduce the MeV bump, we assume that some fraction of the jet is filled with pair plasma, evolving in the same way as the ultrarelativistic component, over a long period of time. We find this fraction to be ~ 10 %. This is consistent with the observation of strong variability in the EGRET regime if one assumes that during the quiescent phases the injection of relativistic pair plasma into the jet is very inefficient, and is in perfect agreement with the typical flaring duty cycle of EGRET detected blazars. The combined inverse-Compton, pair annihilation and pair bremsstrahlung spectrum emitted by the quasi-thermalized pair plasma jet as it moves out and is diluted due to jet expansion and pair annihilation, is shown by the solid line in Fig. 9.

We point out that the MeV bump can be fit with a self-consistent pair annihilation spectrum

only under the assumption of a cylindrical jet, which seems to contradict the assumption that the gas pressure of the pair plasma greatly exceeds the magnetic pressure, most probably responsible for the jet confinement.

6. Summary and conclusions

Motivated by the standard model for γ-ray emission from blazars invoking jets filled with ultrarelativistic pair plasma oriented at a small angle with respect to the line of sight, we investigated the further evolution of the leptonic material inside such a jet after the initial phase in which the high-energy (> 100 MeV) γ-ray radiation is produced.

We demonstrated that either the action of elastic scattering of particles off each other or the balance of reacceleration by turbulent plasma waves to radiative losses can, under a wide range of parameters, establish a quasi-thermal particle distribution inside the jet, irrespective of the initial pair distribution at the time of injection. Extreme conditions (high density, very weak magnetic field, injection close to the accretion disk) are necessary to achieve mildly relativistic temperatures ($\Theta \sim 1$). Radiation from a quasi-thermal pair plasma can produce the temporary MeV bumps observed in MeV blazars. This can be accomplished most easily via inverse-Compton scattering of external soft radiation by a quasi-continuously filled jet.

Alternatively, the MeV bump could be produced by pair annihilation radiation, if cooling of the pair distribution is very efficient and the dilution of the plasma through jet expansion is negligible. We found that only the unrealistic assumption of a cylindrical jet yields an acceptable fit to the observed MeV bump, if the pair plasma producing this bump is subject to the same processes (in the same environment) as the ultrarelativistic pair plasma producing the EGRET spectrum.

In this picture, an MeV outburst reflects an increasing supply of relativistic electrons and positrons into the jet on much longer timescales than those typically observed in EGRET outbursts at higher energies. It is only weakly or not at all correlated to activity in the EGRET range which corresponds to an increased energy density at the acceleration site, leading to a harder particle spectrum of the injected pairs.

If the bulk Compton process is the dominant mechanism for the production of the MeV bump in MeV blazars, then there is no obvious reason for a "universality" of the bump photon energy at 3 — 10 MeV. Mainly depending on the magnetic field strength, the level of hydromagnetic turbulence and the injection height of the plasma blob above the accretion disk, similar sources with bulk-Compton radiation bumps at different energies should exist as well.

In general, our treatment is also applicable to the so-called hadronic jet models, where ultrarelativistic protons initiate a pair cascade in the jet (Mannheim et al. 1991, Mannheim & Biermann 1992, Mannheim 1993). However, although the jet simulation code of BMS is able to

handle problems in which the blob is optically thick to $\gamma\gamma$ pair production, it is clearly beyond the scope of this paper to follow the proton-initiated pair cascades in detail. Nevertheless, a few general conclusions may be drawn from the fact that in those models, the magnetic fields are fairly high and a considerable level of turbulence might be present. Our simulations indicate that at magnetic fields of $B \gtrsim 10$ G, as usually assumed in hadronic jet models, and the moderate pair densities expected to result in the cascades, the pair plasma will maintain a highly relativistic temperature, $\Theta \gtrsim 100$. Thus, no pair annihilation feature will be observable; instead, strong synchrotron and SSC bumps at $\sim 3 \cdot 10^7 \cdot D/(1+z)\,(B/G)\,\Theta^2$ Hz and $\sim 4 \cdot 10^8 \cdot D/(1+z)\,(B/G)\,\Theta^4$ Hz, respectively, would be expected from the thermalized cascade plasma.

We thank the anonymous referee for valuable comments and suggestions which led to significant improvements of the manuscript. This work has been partially supported by NASA grant NAG 5-4055. R. S. acknowledges partial support by the DARA.

A. Energy exchange and dispersion rates

A.1. Energy dispersion due to elastic scattering

Following Dermer (1985), the energy dispersion rate is given by

$$\frac{d(\Delta\gamma)^2}{dt} = 8\pi^2\, N_\pm\, c \int\limits_1^\infty d\gamma_r\, (\gamma_r^2 - 1)$$
$$\int\limits_1^\infty d\gamma_c\, \sqrt{\gamma_c^2 - 1} \int\limits_{-1}^{1} du\, f_1(\gamma_1)\, f_2(\gamma_2)\, \sigma_{Mo}(\gamma_r)\, \left\langle (\Delta\gamma)^2 \right\rangle \tag{A1}$$

where

$$\left\langle (\Delta\gamma)^2 \right\rangle = \frac{2\,\pi\, r_e^2\, (\gamma_c^2 - 1)}{\sigma_{Mo}(\gamma_r)\, \gamma_{cm}^2\, (\gamma_{cm}^2 - 1)} \cdot$$
$$\cdot \Bigg(u^2 \left[\frac{\gamma_r^2}{2} - \left(2\,\gamma_{cm}^4 - \gamma_{cm}^2 - \frac{1}{4} \right) (2\,\ln 2 - 1) + \frac{(\gamma_{cm}^2 - 1)^2}{12} \right]$$
$$+ \frac{[1-u^2]}{2} \left[\gamma_r^2 \left(\frac{1}{2} \ln 2 + \ln \Lambda \right) \right.$$
$$\left. - \left(2\,\gamma_{cm}^4 - \gamma_{cm}^2 - \frac{1}{4} \right) + \frac{(\gamma_{cm}^2 - 1)^2}{6} \right] \Bigg). \tag{A2}$$

Here γ_r is the Lorentz factor of the relative motion of the interacting particles, γ_c is the Lorentz factor (normalized velocity: β_c) of motion of the center-of-momentum (cm) frame with respect

to the blob frame, γ_{cm} is the Lorentz factor (normalized velocity: β_{cm}) of the particles in the center-of-momentum frame, and u is the cm angle cosine between $\overrightarrow{\beta_{cm}}$ and $\overrightarrow{\beta_c}$.

It is accurate within a few percent to retain only the leading terms $\sim u^2$ and $\sim (1-u^2)$, respectively, that is the terms $\sim u^2\,\gamma_r^2/2$ and $\sim (1-u^2)\,\gamma_r^2\,(\ln\sqrt{2}/2 + \ln\Lambda)/2$ in Eq. (6). Nayakshin and Melia (1998) suggested an approximation based on the further neglect of all terms not containing an $\ln\Lambda$, arguing that this contribution is the one resulting from small-angle scatterings and that, at the point where other contributions may become important, the use of the Fokker-Planck equation is no longer a good approach since then large-angle scattering, changing the particles' energy considerably, dominate the energy exchange in elastic scattering events. Our simulations show that in the case of the system we are dealing with the energy distributions of the pairs remain relatively narrow. In this case, the dispersion may indeed be approximated by the expression found by Nayakshin & Melia which ensures the validity of the Fokker-Planck equation. Nevertheless, we retain both contributions ($\sim u^2$ and $\sim [1-u^2]$) in order to see whether large-angle scattering is important at the point where the plasma starts to thermalize (i. e. when elastic scattering becomes the dominant process).

With this simplification, the dispersion rate due to elastic scattering off an isotropic distribution of particles $n_2(\gamma_2)$ is given by

$$\left(\frac{d[\Delta\gamma]^2}{dt}\right)_{Mo} = \int_1^\infty d\gamma_2\; n(\gamma_2)\, D(\gamma,\gamma_2). \tag{A3}$$

where

$$\begin{aligned} D(\gamma_1,\gamma_2) = \frac{4\,\pi\, r_e^2\, c\, n_2}{\gamma_t^2\beta_t\,\gamma_2^2\beta_2}\Bigg\{ &\left(\ln\Lambda + \frac{[\gamma_t-\gamma_2]^2}{4}\,[1-\ln\Lambda]\right)\cdot \\ &\cdot\left(2\,\ln\left[\gamma_{cm}(1+\beta_{cm})\right] + 2\,\gamma_{cm}^2\beta_{cm} - \frac{1}{\beta_{cm}}\right) \\ &+\frac{(\gamma_t+\gamma_2)^2}{2}\left(\gamma_{cm}^2\beta_{cm} + \frac{1}{2}\gamma_{cm} - \ln\left[\gamma_{cm}(1+\beta_{cm})\right]\right) \\ &-\left(\gamma_{cm}^4 + \frac{3}{2}\gamma_{cm}^2\right)\beta_{cm} - \frac{1}{\beta_{cm}} + \frac{5}{2}\ln\left(\gamma_{cm}[1+\beta_{cm}]\right)\Bigg\}\Bigg|_{\gamma_{cm}^{min}}^{\gamma_{cm}^{max}} \end{aligned} \tag{A4}$$

is the monoenergetic dispersion rate and

$$\gamma_{cm}^{min/max} = \sqrt{\frac{1}{2}(1+\gamma_1\gamma_2[1\mp\beta_1\beta_2])}. \tag{A5}$$

A.2. Bremsstrahlung energy loss

Using again the technique of Dermer (1985), we find the single-particle energy loss rate due to pair bremsstrahlung emission to be

$$\left(\frac{d\gamma_t}{dt}\right)_{br} = -\frac{\pi\, N_\pm\, c}{\beta_t\, \gamma_t^2} \int_1^{\gamma_r^{max}} d\gamma_r\, \gamma_r^2\, \beta_r^2 \int_{\gamma_c^{min}}^{\gamma_c^{max}} d\gamma_c\, \frac{f_2\,(2\,\gamma_{cm}\,\gamma_c - \gamma_t)}{\gamma_{cm}\beta_{cm}\,\gamma_c + \gamma_{cm}\,\gamma_c - \gamma_t}\, \overline{K}(\gamma_{cm}) \tag{A6}$$

where

$$\overline{K}(\gamma_{cm}) \equiv \int_0^{\epsilon_{cm}^{max}} d\epsilon_{cm}\, \epsilon_{cm} \left(\frac{d\sigma_{br}}{dk}\right)_{cm} =$$
$$\frac{\alpha\,\sigma_T}{\pi}\,\gamma_{cm}\left\{\beta_{cm}\left(\ln\left[\frac{4\gamma_{cm}}{\beta_{cm}}\right] - \frac{1}{2}\right)\left(4 - 2\,\beta_{cm} + \beta_{cm}^2\right)\right.$$
$$+(1-\beta_{cm})^2\left(\ln[\gamma_{cm}(1-\beta_{cm})] - \frac{1}{2}\right) + \frac{\beta_{cm}^2}{3}\,(3+\beta_{cm})$$
$$-(1-\beta_{cm})\,(3\ln[\gamma_{cm}(1-\beta_{cm})]+1) + 3\ln\gamma_{cm} + \frac{7}{6}$$
$$\left. + (1-\beta_{cm})^3\,\left(\ln[\gamma_{cm}(1-\beta_{cm})] - \frac{1}{3}\right)\right\}\Bigg|_{\gamma_{cm}=\gamma_{cm}^{max}} \tag{A7}$$

(cf. DL). The maximum photon energy ϵ_{cm}^{max} is given by

$$\epsilon_{cm}^{max} = \gamma_{cm}\,\beta_{cm}^2. \tag{A8}$$

A.3. Energy dispersion due to inverse-Compton scattering

The energy dispersion rate due to inverse-Compton scattering of photons of differential density $n_{ph}(\epsilon, \Omega_{ph})$ in the Thomson regime is

$$\left(\frac{d(\Delta\gamma)^2}{dt}\right)_{EIC} = 4\,\pi\,c\,\sigma_T\gamma^2\,\beta^2\left(\gamma^2\,\beta^2 + \frac{1}{6}\right)\cdot$$
$$\cdot \int_{-1}^{1} d\eta_{ph} \int_0^\infty d\epsilon\, \epsilon^2 n_{ph}(\epsilon, \Omega_{ph}) \tag{A9}$$

where η_{ph} is the cosine of the angle between soft photon momentum and jet axis. Inserting the photon number density (I.8) yields

$$\left(\frac{d(\Delta\gamma)^2}{dt}\right)_{EIC} = \frac{48\,\pi\,\sigma_T}{c^2}\Gamma^3\left(\frac{m_e c^2}{h}\right)^3 \zeta(5)\cdot$$
$$\cdot\ \gamma^2\,\beta^2\,\left(\gamma^2\beta^2+\frac{1}{6}\right)\int_{R_i}^{R_a} dR\,\Theta^5(R)\frac{(x-\beta_\Gamma z)^3}{x^5} \tag{A10}$$

where $R_{i/a}$ is the radius of the inner/outer edge of the accregion disk, respectively, $x=\sqrt{R^2+z^2}$ and $\zeta(n)=\sum_{k=1}^{\infty}k^{-n}$.

In the case of an isotropic soft photon field we have $n_{ph}(\epsilon,\Omega_{ph})=n_{ph}(\epsilon)/4\pi$ (e. g. synchrotron photons in our model), and Eq. (19) reduces to

$$\left(\frac{d(\Delta\gamma)^2}{dt}\right)_{SSC} = 2\,c\,\sigma_T\,\gamma^2\beta^2\,\left(\gamma^2\beta^2+\frac{1}{6}\right)\int_0^{\infty} d\epsilon\,\epsilon^2\,n_{sy}(\epsilon). \tag{A11}$$

A.4. Pair annihilation losses

The general expression for the catastrophic particle losses due to pair annihilation can be written as

$$\left(\frac{d\,n_\pm(\gamma,t)}{dt}\right)_{PA} = -n_\mp(\gamma,t)\int_1^{\infty} d\gamma_\mp\,n_\pm(\gamma_\mp)\,\overline{v\sigma}(\gamma_+,\gamma_-) \tag{A12}$$

where

$$\overline{v\sigma}(\gamma_+,\gamma_-) = \frac{c\,\pi\,r_e^2}{\beta_-\gamma_-^2\,\beta_+\gamma_+^2}\cdot$$
$$\cdot\left(\beta_{cm}^3\gamma_{cm}^2 L[\beta_{cm}] - 2\,\gamma_{cm}^2 + \frac{3}{4}\,L^2[\beta_{cm}]\right)\Bigg|_{\gamma_{cm}^{min}}^{\gamma_{cm}^{max}} \tag{A13}$$

is the angle-averaged reaction rate and

$$L(\beta) \equiv \ln\left(\frac{1+\beta}{1-\beta}\right) \tag{A14}$$

(Svensson 1982). γ_{cm}^{min}, γ_{cm}^{max} are given by the kinematic restrictions, namely

$$\sqrt{\frac{1}{2}\left(1+\gamma_1\gamma_2[1-\beta_1\beta_2]\right)} \leq \gamma_{cm} \leq \sqrt{\frac{1}{2}\left(1+\gamma_1\gamma_2[1+\beta_1\beta_2]\right)}. \tag{A15}$$

B. Approximative analytical solution

As we found in section 4, for ultrarelativistic particles with $\gamma \gtrsim 100$, and neglecting pair annihilation, the Focker-Planck equation (1) can be approximated as

$$\frac{1}{\chi(t)}\frac{\partial n}{\partial t} - \frac{\partial}{\partial \gamma}\left(A_1\,\gamma^2\,n + \frac{A_2}{2}\frac{\partial}{\partial \gamma}\left[\gamma^4\,n\right]\right) = 0 \tag{B1}$$

where $n = n(\gamma, t)$ and $\partial n/(\chi[t]\partial t) = \partial n/\partial T$. Laplace transformation of Eq. (B1) to

$$N(\gamma, s) = \int_0^\infty dT\, n(\gamma, t)\, e^{sT} \tag{B2}$$

yields an ordinary differential equation of second order in γ:

$$\phi_0(\gamma)\, N(\gamma) + \phi_1(\gamma)\, N'(\gamma) + \phi_2(\gamma) N''(\gamma) = n(\gamma, 0) \tag{B3}$$

where

$$\phi_0(\gamma) := s - 2\,A_1\,\gamma - 6\,A_2\,\gamma^2, \tag{B4}$$

$$\phi_1(\gamma) := -A_1\,\gamma^2 - 4\,A_2\,\gamma^3, \tag{B5}$$

$$\phi_2(\gamma) := -\frac{A_2}{2}\gamma^4. \tag{B6}$$

Eq. (B3) can be written in the form

$$\left(p[\gamma], N'(\gamma)\right)' - g(\gamma)\, N = -\frac{n(\gamma, 0)}{f(\gamma)} \tag{B7}$$

with

$$p(\gamma) = e^{-\frac{2\,A_1}{A_2\,\gamma}}\,\gamma^8, \tag{B8}$$

$$f(\gamma) = \frac{A_2}{2} e^{\frac{2\,A_1}{A_2\,\gamma}}\,\gamma^{-4}, \tag{B9}$$

$$g(\gamma) = \frac{2}{A_2}\,e^{-\frac{2\,A_1}{A_2\,\gamma}}\,\left(s\,\gamma^4 - 2\,A_1\,\gamma^5 - 6\,A_2\,\gamma^6\right) \tag{B10}$$

In the first step we search for a homogeneous solution $h(\gamma)$ which satisfies the equation

$$\left(p[\gamma]h'\right)' - g(\gamma)\,h = 0. \tag{B11}$$

Substituting

$$h(\gamma) = p(\gamma)^{-1/2}\,P(x), \tag{B12}$$

choosing $x = \gamma^{-1}$ and inserting the functions g and p, yields a differential equation for $P(x)$:

$$x\,P''(x) + 2\,P'(x) - (\zeta\,x + \eta)\,P(x) = 0 \tag{B13}$$

where

$$\zeta = \frac{A_1^2}{A_2^2} + \frac{2\,s}{A_2}, \tag{B14}$$

$$\eta = \frac{2\,A_1}{A_2}. \tag{B15}$$

Two linearly independent solutions of Eq. (B 13) are given by

$$\tilde{P}_1(x) = \frac{1}{x}\,M_{-\frac{\eta}{2\alpha},\,\frac{1}{2}}(2\alpha\,x), \tag{B16}$$

$$\tilde{P}_2(x) = \frac{1}{x}\,W_{-\frac{\eta}{2\alpha},\,\frac{1}{2}}(2\alpha\,x) \tag{B17}$$

where $\alpha = \sqrt{\zeta}$. Since we did not find an analytical solution for the inverse Laplace transformation

$$G(\gamma, \gamma_0, T) = \frac{1}{2\,\pi\,i}\int\limits_{x-i\infty}^{x+i\infty} ds\,e^{Ts} G(\gamma, \gamma_0, s) \tag{B18}$$

of the Green's function resulting from the homogeneous solutions $h_{1/2}(\gamma) = p^{-1/2}(\gamma)\,\tilde{P}_{1/2}(1/\gamma)$ we simplify Eq. (B 13) in a convenient manner. Since the energy loss and dispersion rates are dominated by the inverse-Compton process, we find for the coefficients

$$A_1 \sim c\,\sigma_T \int\limits_0^\infty d\epsilon\,\epsilon\,n_{ph}(\epsilon), \tag{B19}$$

$$A_2 \sim c\,\sigma_T \int\limits_0^\infty d\epsilon\;\epsilon^2\,n_{ph}(\epsilon) \tag{B20}$$

where ϵ and $n_{ph}(\epsilon)$ are dimensionless energy and spectral photon number of the accretion disk photon field in the blob rest frame. Hence, we can estimate

$$\frac{A_1}{A_2} \sim \frac{1}{\langle\epsilon\rangle} \sim 10^5 \tag{B21}$$

for the accretion disk model we used (see BMS, section 2.1). Since for the Laplace transform $\Re s > 0$, we have $|\zeta| \gtrsim 10^{10}$ and $\eta \sim 10^5$. Thus, for particle energies $\gamma \lesssim 10^4$, $\zeta x \gg \eta$, and we may neglect the term $\sim \eta$. The numerical values for the coefficients A_1 and A_2 which we find during our simulations confirm the above estimate. Therefore, Eq. (B 13) is well approximated by

$$P''(x) + \frac{2}{x}P'(x) - \zeta\,P(x) = 0 \tag{B22}$$

which is solved by

$$P_{1/2}(x) = \frac{1}{x}\,e^{\pm\alpha x} \tag{B23}$$

where, again $\alpha = \sqrt{\zeta}$. The homogeneous solutions are thus

$$h_{1/2}(\gamma) = e^{\left(\frac{A_1}{A_2\gamma}\pm\alpha\right)\frac{1}{\gamma}}\,\gamma^{-3}. \tag{B24}$$

The Laplace-transformed Green's function $G(\gamma,\gamma_0,s)$ is then constructed as

$$G(\gamma,\gamma_0,s) = \frac{1}{C}\cdot$$
$$\cdot\,\Big\{\Theta(\gamma_0-\gamma)\,h_1(\gamma)\,h_2(\gamma_0) + \Theta(\gamma-\gamma_0)\,h_2(\gamma)\,h_1(\gamma_0)\Big\} \tag{B25}$$

where

$$C = p(\gamma)\,W\{h_1,h_2\}(\gamma) = 2\,\alpha \tag{B26}$$

and $W\{h_1,h_2\}$ denotes the Wronskian. The functions h_1 and h_2 are chosen in a way that h_1 fullfills the boundary condition at $\gamma \to 1$ and h_2 fullfills the boundary condition for $\gamma \to \infty$ where we simply have to use the condition of finite solutions $G(\gamma,\gamma_0,s)/f(\gamma_0)$ at $\gamma \to \infty$ and $\gamma \ll \alpha$. (In the approach used here we can also write Eq. (B1) differential in kinetic energy $E := \gamma - 1$ yielding the same solution in E instead of γ; then the boundary condition is determined by a finite value of G/f at $E = 0$.) Thus, the resulting Laplace transformed Green's function is

$$G(\gamma,\gamma_0,s) = -\frac{e^{\frac{A_1}{A_2}\left(\frac{1}{\gamma}+\frac{1}{\gamma_0}\right)}}{2\,\alpha\,\gamma^3\,\gamma_0^3}\,e^{-\alpha\left|\frac{1}{\gamma_0}-\frac{1}{\gamma}\right|}. \tag{B27}$$

The inverse Laplace transform of this Green's function is

$$G(\gamma,\gamma_0,T) = \\ -\frac{e^{\frac{A_1}{A_2}\left(\frac{1}{\gamma}+\frac{1}{\gamma_0}\right)}}{4\,\gamma^3\gamma_0^3}\,\frac{A_2\,e^{-\frac{A_1^2}{2\,A_2}T}}{\sqrt{\pi\,A_2\,\frac{T}{2}}}\,e^{-\left(\frac{1}{\gamma_0}-\frac{1}{\gamma}\right)^2/(2\,A_2\,T)}, \tag{B28}$$

and an approximative solution of Eq. (B 1) is given by

$$n(\gamma,T) = -\int_1^\infty d\gamma_0\,G(\gamma,\gamma_0,T)\,\frac{n(\gamma_0,0)}{f(\gamma_0)} \\ = \frac{e^{\frac{A_1}{A_2\gamma}-\frac{A_1^2}{2A_2}T}}{2\,\gamma^3\,\sqrt{\pi\,A_2\,T/2}}\cdot \\ \cdot\int_1^\infty d\gamma_0\,n(\gamma_0,0)\,\gamma_0\,e^{-\frac{A_1}{A_2\gamma_0}}\,e^{-\left(\frac{1}{\gamma_0}-\frac{1}{\gamma}\right)^2/(2\,A_2\,T)}. \tag{B29}$$

REFERENCES

Barthel P.D. et al., 1995, ApJ 444, L21

Blandford, R. D., & Rees, M. J., 1974, MNRAS 169, 395

Blandford, R. D., & Königl, A., 1979, ApJ 232, 34

Bloemen, H., Bennett, K., Blom, J. J., et al., 1995, A&A 293, L1

Blom, J. J., Bennett, K., Bloemen, H., et al., 1995, A&A 298, L33

Blom, J. J., 1996, Proceedings of the Heidelberg Workshop on Gamma-Ray Emitting AGN, Eds. J.G. Kirk et al., MPI H-V37-1996, p.33

Böttcher, M. & Schlickeiser, R., 1995, A&A 302, L17

Böttcher, M. & Schlickeiser, R., 1996, A&A 306, 86

Böttcher, M., Mause, H., & Schlickeiser, R., 1997, A&A 324, 395 (BMS)

Collmar et al., 1997, A&A 328, 33

Crusius, A. & Schlickeiser, R., 1988, A&A 196, 327

Dermer, C. D., 1984, ApJ 280, 328

Dermer, C. D., 1985, ApJ 295, 28

Dermer, C. D., Gehrels N., 1995, ApJ 447, 103

Haug, E., 1975, Zeitschrift. f. Naturforschung, 30 a, 1099

Haug, E., 1985a, Phys. Rev. D, 31, 2120

Haug, E., 1985b, A&A 148, 386

Henri, G., Pelletier, G., Roland, J., 1993, ApJ 404, L41

Krichbaum T.P. et al., 1995, in *Quasars and AGN*, Eds. M. Cohen & K. Kellermann, Proc. Nat. Acad. Sci. 92, 11377

Mannheim, K., Biermann, P. L., & Krülls, W. M., 1991, A&A 251, 723

Mannheim, K., & Biermann, P. L., 1992, A&A 253, L21,

Mannheim, K., 1993, A&A 269, 67

Marcowith, A., Henri, G., Pelletier, G., 1995, MNRAS 277, 681

McNaron-Brown K. et al., 1995, ApJ 451, 575

Montigny C. von, et al. 1995, ApJ 440, 525

Mukherjee R. et al., 1997, ApJ 490, 116

Mücke A. et al., 1997, A&A 320, 33

Mücke A. et al., 1996, A&AS 120, C541

Nayakshin, S., Melia, F., 1998, ApJS 114, 269

Pohl M. et al., 1995, A&A 303, 383

Pohl M. et al., 1997, A&A 326, 51

Pohl M., 1996, A&AS 120, C457

Roland J., Hermsen W., 1995, A&A 297, L9

Schlickeiser, R., 1985, A&A 143, 431

Schlickeiser, R., 1989, ApJ 336, 243

Schlickeiser, R., 1996, A&AS 120, C481

Sikora, M.,, Madejski, G., Moderski, R., Poutanen, J. 1997, ApJ, 484, 108

Skibo, J. G., Dermer, C. D., Ramaty, R., McKinley, J. M., 1995, ApJ **446**, 86

Stacy J.G. et al., 1996, A&AS 120, C549

Thompson D.J. et al., 1995, ApJS 101, 259

Wehrle A.E. et al., 1994, in *The Multimission Perspective*, Eureka Scientific, Napa Valley, p.27

Williams O.R. et al., 1995, A&A 298, 33

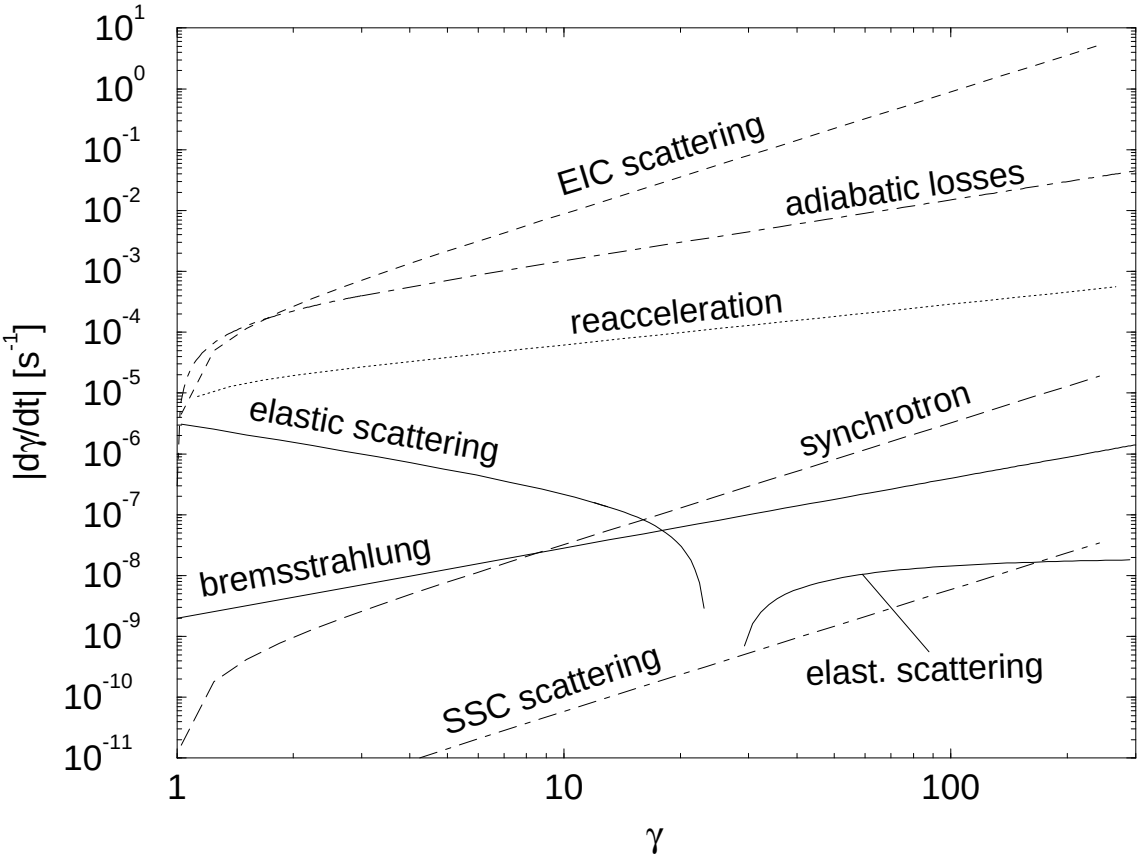

Fig. 1.— Energy-loss rates in a dense relativistic jet for the following parameters: $n = 3 \cdot 10^6\,\mathrm{cm}^{-3}$, $\langle\gamma\rangle \approx 30$, $B_0 = 0.1$ G, $\delta B/B_0 = 0.1$, $z = 10^{-3}$ pc, $L_0 = 10^{46}\,\mathrm{erg\,s}^{-1}$, $\Gamma = 15$

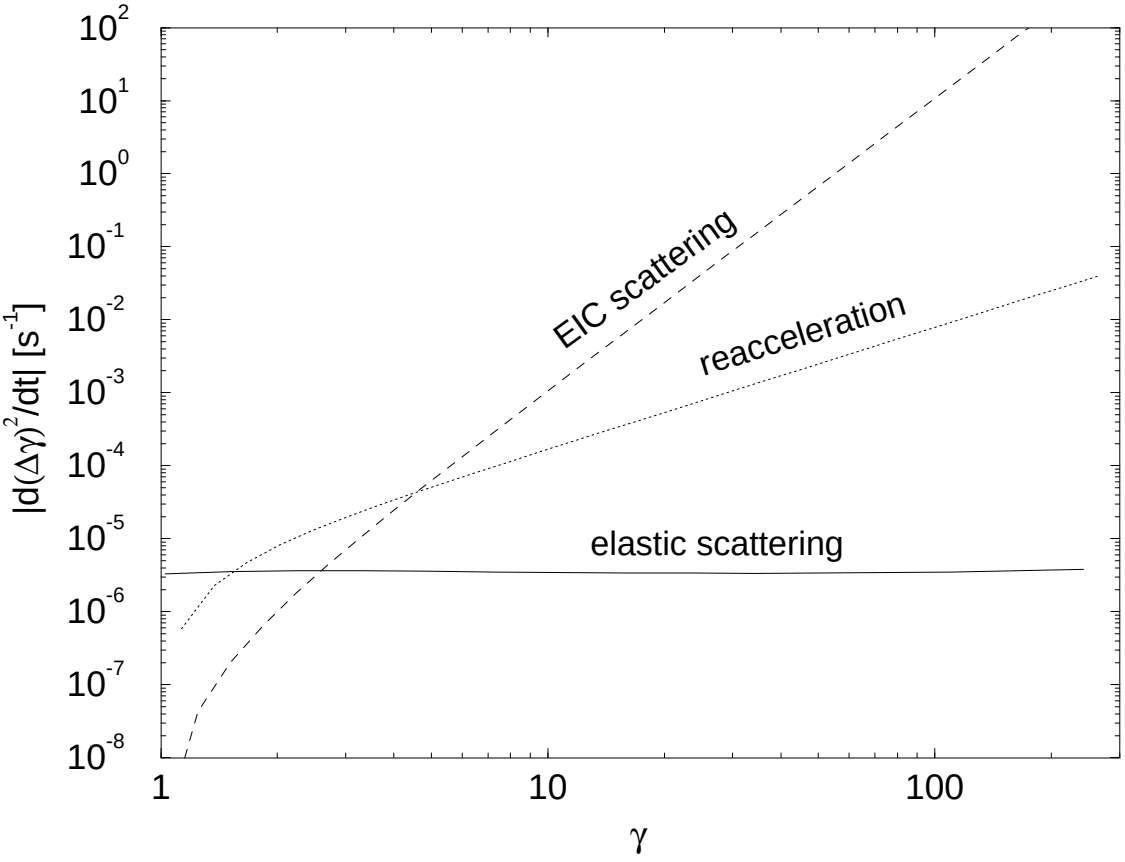

Fig. 2.— Energy-dispersion rates in a dense relativistic jet for the same set of parameters as in Fig. 1

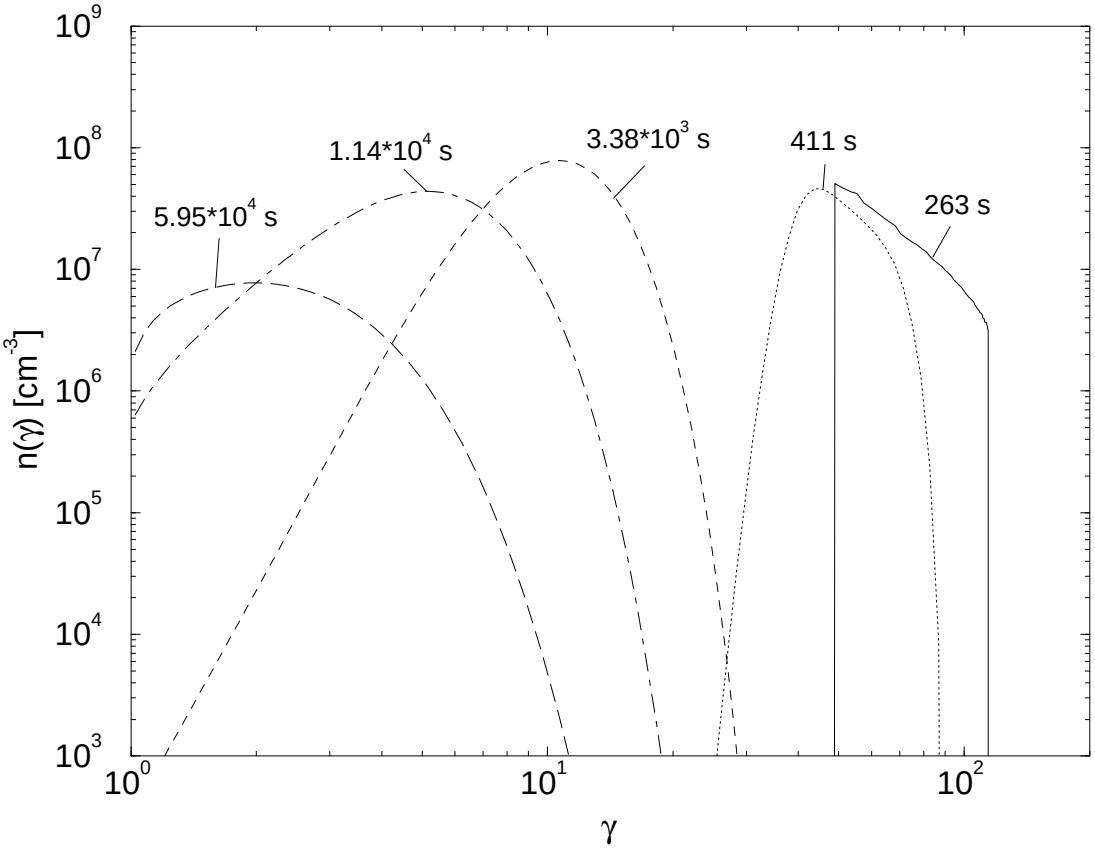

Fig. 3.— Evolution of the pair distribution functions through the transrelativistic phase in the case of high particle density, $n_0 = 10^9$ cm^{-3}. Initial conditions: $\gamma_{1\pm} = 200$, $\gamma_{2\pm} = 2 \cdot 10^4$, $s = 2$, $R_B = 5 \cdot 10^{12}$ cm, $B_0 = 1$ G, $z_i = 10^{-3}$ pc; $L_0 = 10^{46}$ erg s^{-1}, $M = 10^8\, M_\odot$, $\Gamma = 10$. The solid line indicates the state of the plasma after the ultrarelativistic treatment described in BMS

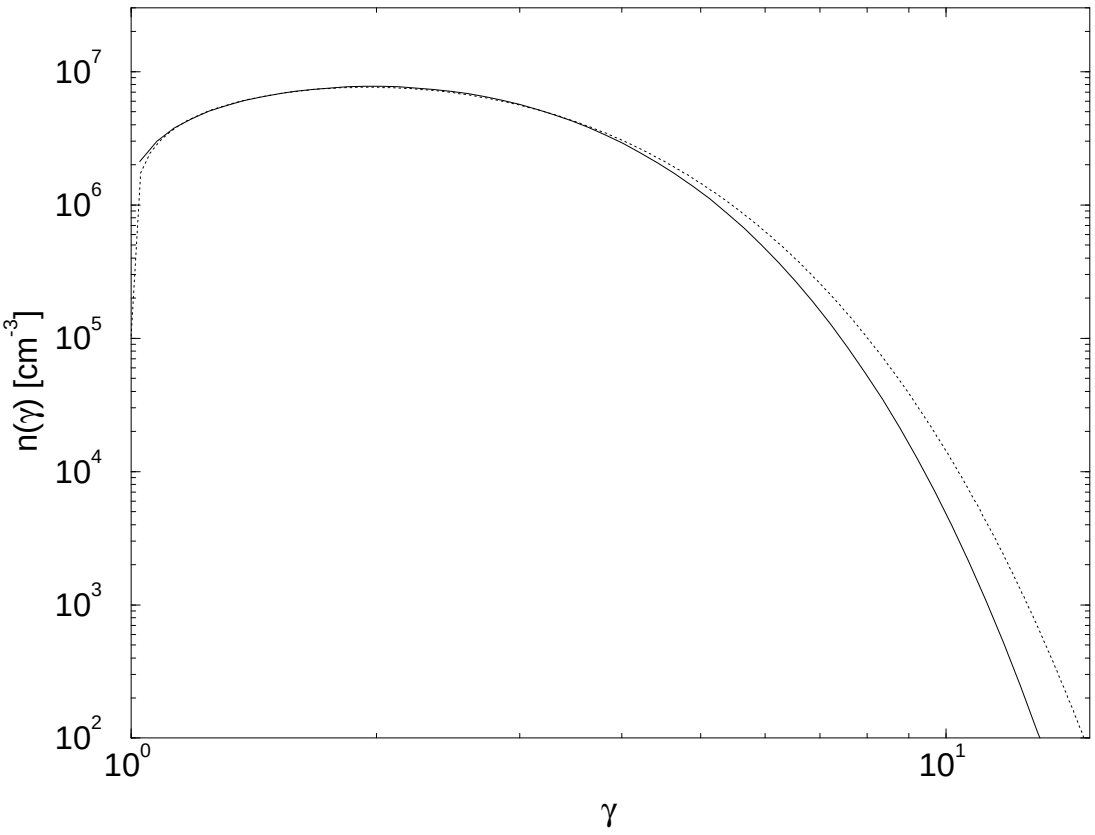

Fig. 4.— Comparison of the final state of the simulation shown in Fig. 3 (solid) to a thermal spectrum of temperature $\Theta = 0.83$ (dotted)

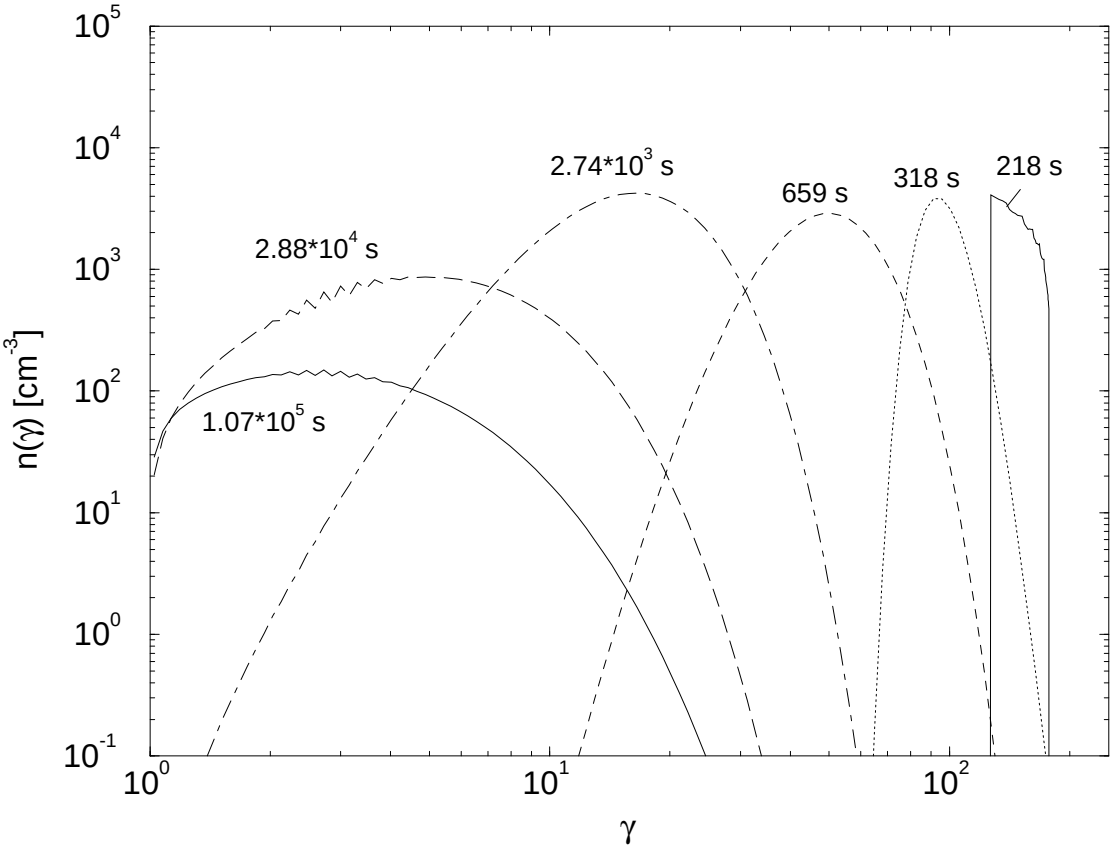

Fig. 5.— Evolution of the pair distribution functions through the transrelativistic phase in the case of moderate particle density, $n_0 = 10^5$ cm^{-3}. Initial conditions: $\gamma_{1\pm} = 500$, $\gamma_{2\pm} = 3 \cdot 10^4$, $s = 2.1$, $R_B = 2 \cdot 10^{15}$ cm, $B_0 = 1$ G, $z_i = 10^{-3}$ pc; $L_0 = 10^{46}$ erg s^{-1}, $M = 10^8\, M_\odot$, $\Gamma = 10$. The solid line indicates the state of the plasma after the ultrarelativistic treatment described in BMS

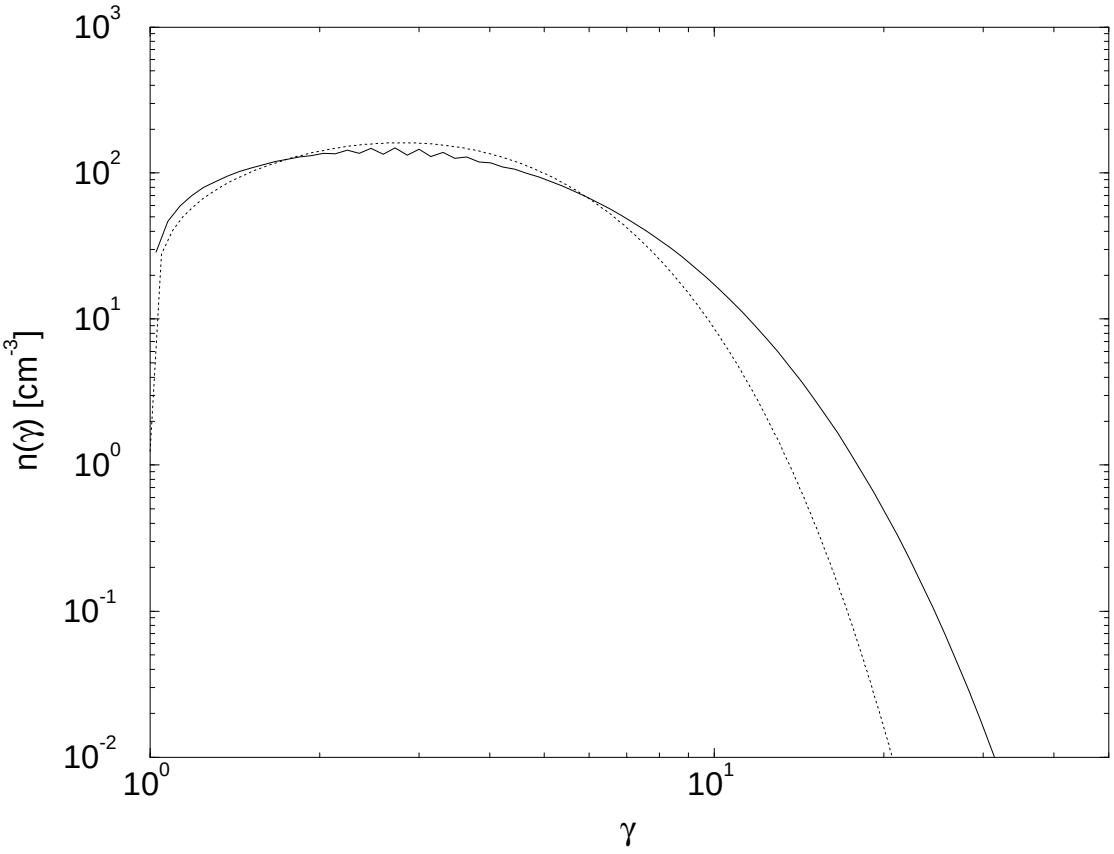

Fig. 6.— Comparison of the final state of the simulation shown in Fig. 5 (solid) to a thermal spectrum of temperature $\Theta = 1.3$ (dotted)

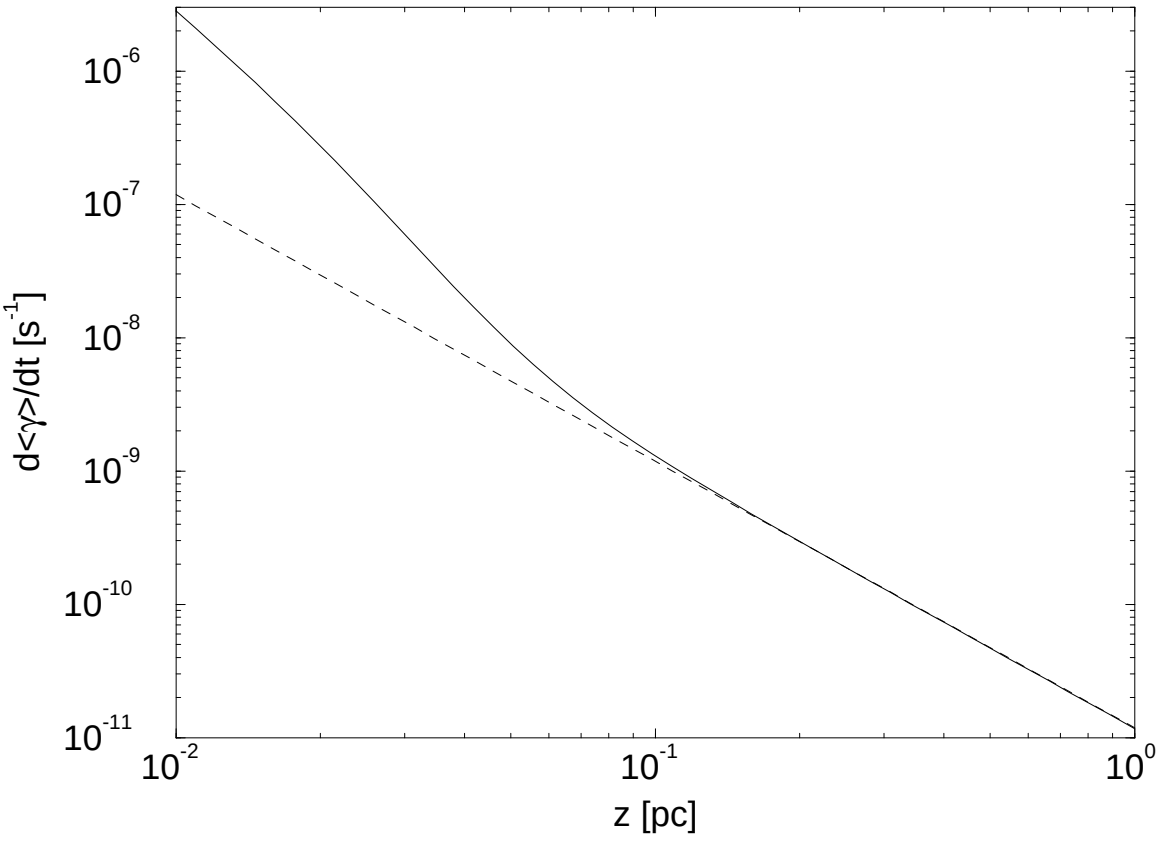

Fig. 7.— Cooling rates of a thermal pair plasma due to inverse-Compton scattering of accretion disk photons as a function of distance from the disk. Solid: Extended source; dashed: point source approximation. $L = 10^{46}$ erg s^{-1}, $M = 10^8\,M_\odot$, $\Theta = 2$

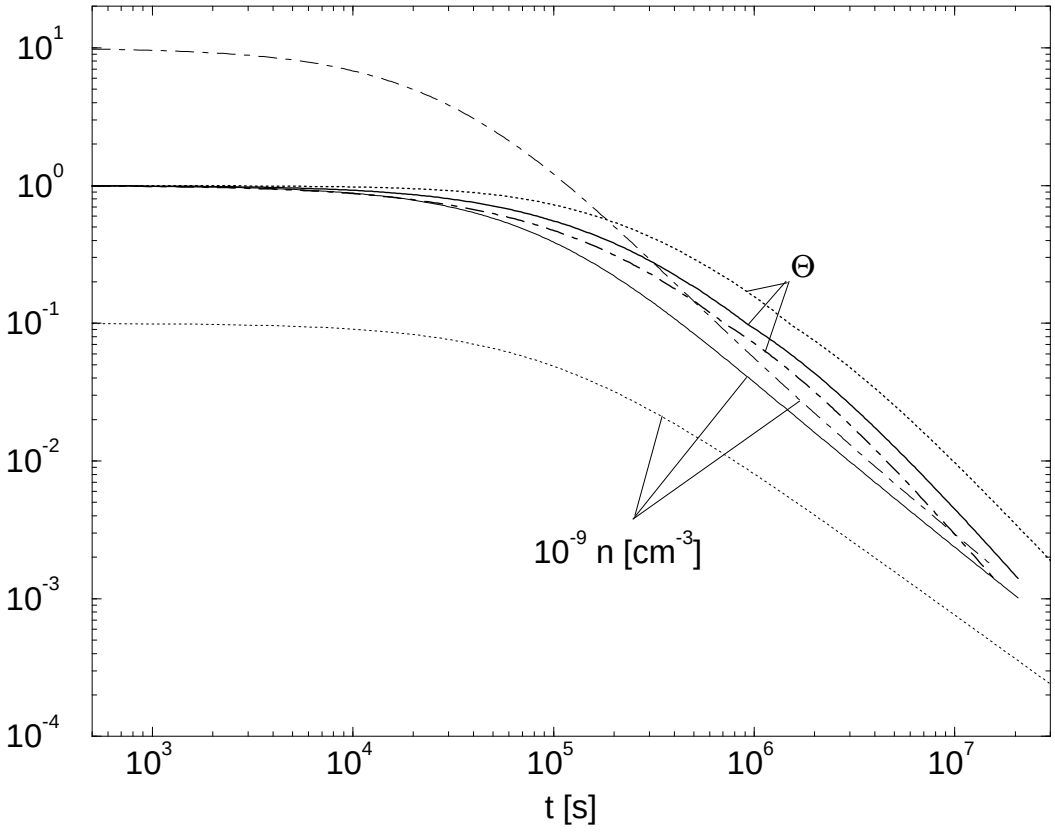

Fig. 8.— Evolution of thermal pair plasmas in a relativistic jet. Initial temperature $\Theta_0 = 1$; $B_0 = 0.1$ G, $z_0 = 10^{-2}$ pc, $L_0 = 10^{46}$ erg s^{-1}, $\Gamma = 10$, $\delta B/B_0 = 0.1$, $B(z) \propto z^{-1}$; initial densities $n_0 = 10^8$ cm^{-3} (dotted), 10^9 cm^{-3} (solid), and 10^{10} cm^{-3} (dot-dashed), respectively. Thick curves show the temperature evolution, thin curves the density (multiplied by 10^{-9})

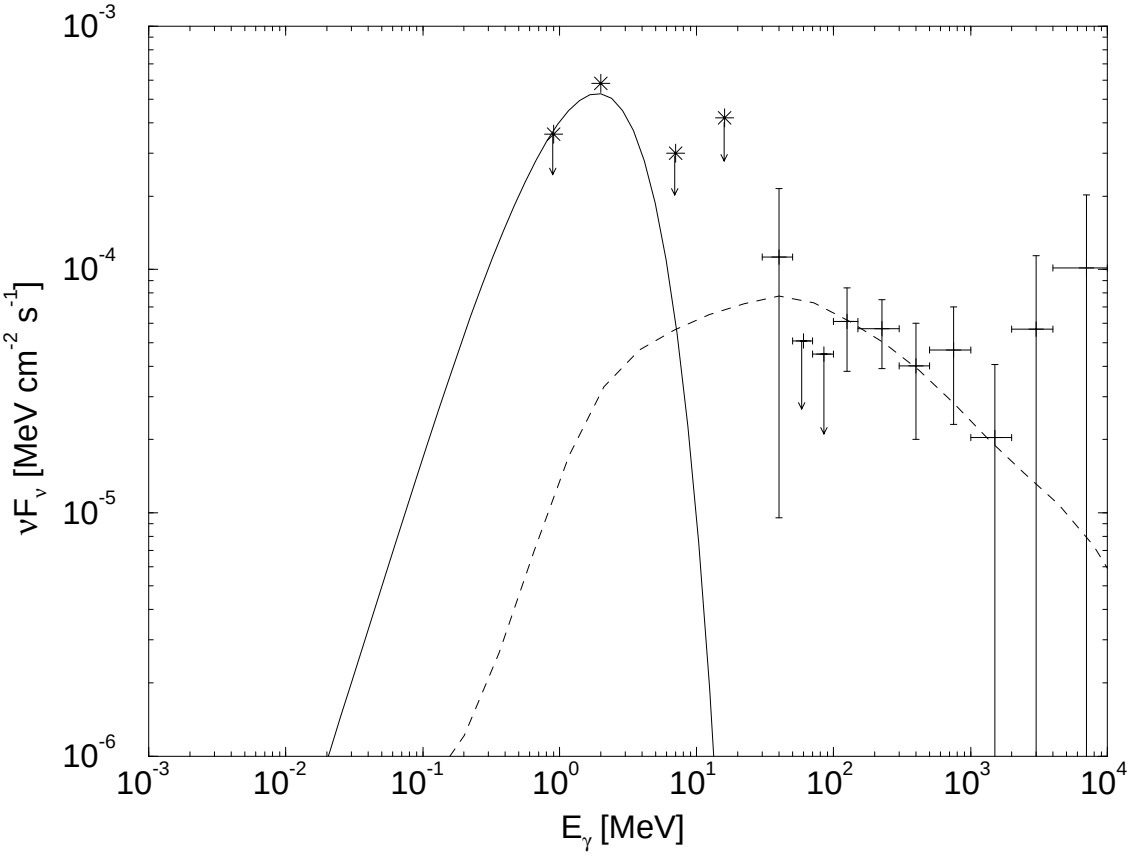

Fig. 9.— The COMPTEL and EGRET spectrum of PKS 0208-512 during Phase II. Dashed: high-energy (predominantly external inverse-Compton) spectrum from ultrarelativistic plasma blobs; solid: inverse-Compton spectrum from the later stages of the jet evolution, under the assumption of ~ 10 % of the jet being filled with transrelativistic pair plasma